KAUNO TECHNOLOGIJOS UNIVERSITETAS

KRISTINA VASILIAUSKIENĖ

MAJENITO DARINIŲ IŠ KATOITO SINTEZĖ, SAVYBĖS IR PANAUDOJIMAS

Daktaro disertacija
Technologiniai mokslai, chemijos inžinerija (T 005)

2024, Kaunas

Disertacija rengta 2019–2023 metais Kauno technologijos universiteto Cheminės technologijos fakultete, Silikatų technologijos katedroje.

Mokslinis vadovas
doc. dr. Anatolijus EISINAS (Kauno technologijos universitetas, technologiniai mokslai, chemijos inžinerija, T 005).

Redagavo: lietuvių kalbos redaktorė Aurelija Gražina Rukšaitė (leidykla „Technologija"), anglų kalbos redaktorė Dovilė Blaudžiūnienė (leidykla „Technologija")

Chemijos inžinerijos mokslo krypties disertacijos gynimo taryba:
prof. dr. Raimundas ŠIAUČIŪNAS (Kauno technologijos universitetas, technologijos mokslai, chemijos inžinerija – T 005) – pirmininkas;
prof. dr. E. VALATKA. (Kauno technologijos universitetas, technologijos mokslai, chemijos inžinerija – T 005);
doc. dr. Irmantas BARAUSKAS (Kauno technologijos universitetas, technologijos mokslai, chemijos inžinerija – T 005);
prof. dr. Jūratė KUMPIENĖ (Lulėjos technologijos universitetas, Švedija, technologijos mokslai, medžiagų inžinerija, T 008),
prof. habil. dr. Aivaras KAREIVA (Vilniaus universitetas, gamtos mokslai, chemija, P 003).

Disertacija bus ginama viešame Chemijos inžinerijos mokslo krypties disertacijos gynimo tarybos posėdyje 2024 m. gegužės 10 d., 10 val. Kauno technologijos universiteto Rektorato salėje.

Adresas: Donelaičio g. 73-402, Kaunas, Lietuva.
Tel. (+370) 608 28 527; el. paštas doktorantura@ktu.lt

Disertacija išsiųsta 2024 m. vasario 26 d.
Su disertacija galima susipažinti interneto svetainėje http://ktu.edu ir Kauno technologijos universiteto bibliotekoje (Gedimino g. 50, Kaunas LT-44239).

KAUNAS UNIVERSITY OF TECHNOLOGY

KRISTINA VASILIAUSKIENE

SYNTHESIS, PROPERTIES AND APPLICATION OF MAYENITE DERIVATES FROM KATOITE

Doctoral dissertation
Technological Sciences, Chemical Engineering (T 005)

2024, Kaunas

This doctoral dissertation was prepared at Kaunas University of Technology, Faculty of Chemical Technology, Department of Silicate Technology during the period of 2019–2023.

Scientific Supervisor

Doc. Dr. Anatolijus EISINAS (Kaunas University of Technology, Technological Sciences, Chemical Engineering, T 005).

Edited by: English language editor Dovilė Blaudžiūnienė (Publishing House "Technologija"), Lithuanian language editor Aurelija Gražina Rukšaitė (Publishing House "Technologija").

Dissertation Defence Board of Chemical Engineering Science Field:

Prof. Dr. Raimundas ŠIAUČIŪNAS (Kaunas University of Technology, Technological Sciences, Chemical Engineering, T 005) – chairperson

Prof. Dr. Eugenijus VALATKA (Kaunas University of Technology, Technological Sciences, Chemical Engineering, T 005).

Prof. Habil. Dr. Aivaras KAREIVA (Vilnius University, Natural Sciences, Chemistry, P 003);

Prof. dr. Jūratė KUMPIENĖ (Luleå University of Technology, Sweden, Technological Sciences, materials engineering, T 008);

Doc. dr. Irmantas BARAUSKAS (Kaunas University of Technology, Technological Sciences, Chemical Engineering, T 005).

The official defence of the dissertation will be held at 10 a.m. on 10 May, 2024 at the public meeting of the Dissertation Defence Board of Chemical Engineering Science Field in Rector's Hall at Kaunas University of Technology.

Address: Donelaičio str. 73-402, Kaunas, Lithuania.
Phone (+370) 608 28 527; email doktorantura@ktu.lt

The doctoral dissertation was sent out on 26 February 2024.
The doctoral dissertation is available on the internet at http://ktu.edu and at the library of Kaunas University of Technology (Donelaičio 20, Kaunas LT-44239, Lithuania).

5. SUMMARY

5.1 Introduction

Recently, the synthesis, structure, and applications of calcium aluminate – mayenite ($12CaO \cdot 7Al_2O_3$) have received considerable attention in the scientific literature. Its unique properties have attracted the attention of researchers, which lead to a wide range of applications: an accelerating effect on cement hydration, ionic conductivity, adsorption capacity for pollutants and the best catalytic properties compared to other compounds of the calcium aluminate group. Mayenite is also a component of environmentally friendly calcium aluminate and calcium sulfoaluminate cements.

The application of mayenite depends on the applied method of synthesis. All methods currently used for the synthesis of mayenite can be divided into three broad groups, which are characterized by the same recurring regularity. One of the most widely used and oldest synthesis methods is the solid-state sintering of the initial mixture at high temperatures (900–1700°C), which takes place during the reaction of calcium oxide and aluminum oxide mixture. This process usually uses a mixture of portlandite ($Ca(OH)_2$) or calcite ($CaCO_3$) and aluminum hydroxide as the starting material. However, mayenite produced by this method has a lower specific surface area, low reactivity and porosity compared to mayenite produced by other synthesis methods. Another widely used synthesis method, such as sol-gel and related methods, has the main distinctive feature that synthesis products are formed by crystallisation from solutions. Although the sol-gel synthesis method can be used to obtain mayenite in a wide range of compositions, it has a number of drawbacks: the use of expensive starting compounds containing calcium and aluminium elements, which must be soluble in the reaction medium, and the multi-step process of both precursor production and purification. It is also inconvenient because the synthesis requires a large amount of expensive solvents and often produces synthesis and/or degradation by-products, which require additional technology and facilities for their isolation/utilisation.

The third group includes two-stage production methods such as the synthesis of calcium hydroaluminate precursors of mayenite and the heat treatment of the resulting products to form the target synthesis product. In the first stage, hydrothermal and/or microwave fusion are commonly used. The properties of the resulting products depend not only on the composition of the starting mixture but also on the choice of synthesis parameters. During heat treatment, it is possible to control the rate of temperature rise, isothermal retention temperature and duration, all of which allow control over the structure and physical parameters of the synthetic mayenite during both hydrothermal and thermal synthesis. This technology has been applied to the synthesis of mayenite, but the scientific literature provides only fragmentary data, often without continuity.

For this reason, the first step is to investigate the influence of the two-stage synthesis conditions on the formation and properties of mayenite. The resulting

synthetic mayenite is likely to be highly reactive and its structural parameters (specific surface area, crystallinity, particle size and pore shape) are likely to be controlled during synthesis. Controlling the properties during production would allow mayenite to be used in wide range of application, for example as an additive in cement, catalysis or adsorption processes. This is very relevant for the reduction of the cement content in concrete and the use of various technogenic wastes and/or natural raw materials in concrete production, in order to reduce CO_2 emissions and to make it cheaper to produce. However, in these systems the initial strength of the cementitious stone is reduced and the hydration process is prolonged, so that a positive and controlled effect of this synthetic additive would allow to accelerate the hydration of both virgin and compound cements.

Another very topical application of synthetic mayenite is the purification of aqueous solutions by adsorption of ionic/anionic contaminants. The literature reports that mayenite adsorbs organic pollutants very efficiently, but studies on its use in aqueous solutions of inorganic cations/anions are limited. The adsorption of Cu^{2+} and SO_4^{2-} ions will be a major focus of this work, as both copper, a heavy metal widely used in industry and subsequently found in wastewaters, and SO_4^{2-}, one of the more difficult cations to treat, also have a high prevalence in industrial wastewaters.

After sorption in aqueous solutions, it is likely that some of the mayenite will directly hydrate to form calcium hydroaluminates, which after heat treatment will form calcium aluminate phases that are active for re-hydration, and thus the activated adsorbent will be suitable for the second adsorption cycle. This would increase the maximum adsorption capacity of pollutants. In order to fully utilize the inorganic cation/anion pollutants the adsorbent could be used as an additive to Portland cement.

The aim of the dissertation is to determine the influence of two-stage synthesis conditions on the formation and properties of mayenite derivatives and propose rational areas of applications

The goals of this work are:
1. To determine the influence of the initial CaO/Al_2O_3 molar ratio and the duration of hydrothermal synthesis on the formation of katoite and its stability at 130°C.
2. To investigate the effect of the combustion temperature of katoite on the formation of mayenite derivatives, their stable existence over temperature ranges and structural properties.
3. To investigate the influence of the additive of synthetic mayenite derivatives on the heat release during early hydration of Portland cement and the mineral composition of the resulting products.
4. Determine the influence of the conditions of synthesis of mayenite derivatives on its adsorption capacity for Cu^{2+}/SO_4^{2-} ions at different initial concentrations of copper sulfate in aqueous solutions.
5. To investigate the effect of activation temperature on the adsorption capacity of Cu^{2+} and SO_4^{2-} ions during repeated adsorption cycles.
6. To develop a heat balance for the mayenite production process based on the best experimental conditions obtained.

Statements presented for the defense

1. Increasing the combustion temperature (from 350 to 900°C) increases the specific surface area and pore volume of the mayenite derivatives almost threefold, and changes the predominant pore shape from a slit between parallel planes to a cylindrical one.
2. The additive of mayenite derivatives, irrespective of the temperature at which it is obtained, modifies the hydration process of Portland cement: promotes calcium sulphate dihydrate reacting, the formation of ettringite, and increases the total amount of heat released.

Scientific novelty of the research

1. The additive of mayenite derivatives obtained under different conditions was found to influence the hydration mechanism of Portland cement, since only the mayenite derivative obtained at 550°C reacts with ettringite and water after a period of wetting in a new exothermic reaction.
2. It was determined that the total adsorption capacity of synthetic mayenite derivatives for Cu^{2+} and SO_4^{2-} ions increases with increasing combustion temperature of the mayenite derivatives and the initial concentration of copper sulphate solution.

Practical significance of the scientific research

For the first time, it has been shown that, after thermal activation, mayenite derivatives can be used for the re-adsorption of Cu^{2+} and SO_4^{2-} ions from aqueous solutions. It has been investigated that the products obtained after two cycles of adsorption and additional heat treatment can be used as accelerators for the hydration process of Portland cement.

Approval and publication of the research results

The results of the research were published in 3 scientific publications in journals indexed in the Web of Science with Impact Factor (JCR SCIE). The results of the dissertation have been reported in 8 international conference proceedings or abstracts.

Contribution of the author and co-authors

The author synthesized and described all the compounds described in the thesis. She also studied the physical, thermal and adsorptive properties of the synthesized compounds, performed mathematical calculations of data reliability and specific surface area, microcalorimetry tests and the effect of the synthesised additive on the early hydration of Portland cement. Anatolijus Eisinas advised on the formation of calcium hydroaluminates by hydrothermal synthesis, the formation of mayenite by heat treatment, the design of the plan, the sequence of experiments and the preparation of the manuscript.

Structure and contents of the dissertation

The dissertation consists of an introduction, a literature review, an experimental part, results and discussion, conclusions, a list of references, a list of publications on the topic of the dissertation. The list of references includes 165 bibliographic sources. The main results are discussed in 153 pages and illustrated in 29 tables and 79 figures.

5.2 MATERIALS AND METHODS

Materials

1. $Ca(OH)_2$ (Sigma-Aldrich, Germany; additionally burned at 550°C for 1.5 h), the quantity of free CaO = 92 wt%, S_a = 1341 m^2/kg.

2. $Al(OH)_3$ (Sigma-Aldrich, Germany) was additionally burned at 475°C (4 h), S_a = 1129 m^2/kg.

3. OPC was manufactured by grinding a mixture of 95.5 wt% clinker (Akmenės cementas, Lithuania) with 4.5 wt% $CaSO_4 \cdot 2H_2O$ (Sigma-Aldrich, Germany), OPC specific surface area was equal 450 m^2/kg. The composition of OPC (tricalcium silicate = 63.19%; dicalcium silicate = 8.89%; tricalcium aluminate = 7.21%; brownmillerite = 12.81%).

4. Quartz sand ("Anykščių kvarcas") ground for 30 min in a vibrating disk mill at a frequency of 900 rpm, specific surface area = 298 m^2/kg, SiO_2 = 99.5%.

5. $CuSO_4 \cdot 5H_2O$, Reachem, Slovakia, purity 99%. Four aqueous solutions were prepared from the salt granules, in which the concentration of Cu^{2+} ions corresponded to 0.5, 1, 3, and 5 g/l.

6. Other pure chemical reagents: HCL (1:1), acetone, ethanol.

Methods

Preparation of initial mixtures and hydrothermal synthesis conditions. The required amount of CaO and Al_2O_3 (molar ratio of CaO/Al_2O_3 = 1.7, 2.8-3.2) was homogenized for 45 min at 49 rpm in a Turbula Type T2F homogenizer (Artisan Technology Group, Czech Republic). The mixture was mixed with H_2O to reach the H_2O/solid ratio by mass value of 10. The synthesis of katoite was performed by the hydrothermal method: in PTFE cells (25 ml) which were added in a stainless-steel autoclave (Parr Instruments, Germany) under saturated steam pressure at a temperature of 130°C for 1–72 val. The isothermal condition was reached within 2 h. After hydrothermal treatment, the samples were rinsed with ethanol and dried (for 24 h) at 50°C temperature.

The determination of free CaO. In fact, 1 g of the sample was weighed and placed into a 250 cm^3 conical flask, poured with 150 cm^3 of distilled water, and 5–10 pieces of glass beads were added. The slurry was heated for 5 minutes. After that, the suspension was cooled down, the inner wall of the flask was sprayed with distilled water, and 2–3 drops of phenolphthalein indicator were added. Finally, the suspension was titrated with 1N HCl, until the pink color disappeared. The amount of free CaO (X) in the sample was calculated by using the following equation:

$$X = \frac{V \cdot N \cdot 28.04 \cdot 100}{G \cdot 1000}; \qquad (5.1)$$

where N is the normality of HCl; V is the volume of titrated HCl, cm^3; 28.04 is CaO equivalent, g; G is the initial mass of the sample, g.

The amount of portlandite was determined by quantitative XRD analysis. The quantity of portlandite was calculated from the intensity change of the basic reflection (0.261 nm). Each calculation was done five times, and it was determined that their data declined no more than ±2% from the mean. Repetition of the measurements (3 time) showed deviations in total heat below 2% for samples of similar type and the heat evolution rates were essentially identical. The function between the main diffraction maximum area of $Ca(OH)_2$ (d-spacing – 0.261 nm) and the quantity of $Ca(OH)_2$ (from 0 to 12% by mass) in the mixtures with quartz was determined. The quantity of portlandite was calculated from a linear equation where $R^2 = 0.9855$.

The X-ray diffraction analysis. The X-ray diffraction (XRD) powder analysis of the samples was performed on the D8 Advance diffractometer (Bruker AXS, Karlsruhe, Germany) operating at the tube voltage of 40 kV and tube current of 40 mA. The X-ray beam was filtered with Ni 0.02 mm filter to select the CuKα wavelength. The diffraction patterns were recorded in a Bragg–Brentano geometry, using a fast counting detector Bruker LynxEye based on the silicon strip technology. The specimens were scanned over the range of 3–70° (2 θ) at a scanning speed of 6°/min, using a coupled two theta/theta scan type. In Situ XRD analysis was made with a high-temperature camera MTC-hightemp (Bruker AXS, Germany). The measurements were carried out with a step width of 0.02 2θ and 0.6 s/step at the heating rate of 50°C/min after the equilibration for 5 min at the desired temperature.

The Fluorescence Spectroscopy (XRF) analysis. Fluorescence Spectroscopy (XRF) performed on a Bruker X-ray S8 Tiger WD (Germany) spectrometer equipped with a Rh tube with the energy of up to 60 keV. Powder samples (passed through a 63 μm sieve and pressed to cylindrical tablets of 5×40 mm) were measured in He atmosphere, and the data was analyzed with SPECTRAPlus QUANT EXPRESS standardless software.

Simultaneous thermal analysis (STA). STA (differential scanning calorimetry (DSC) and thermogravimetry (TG)) was employed for measuring the thermal stability and phase transformation of samples. The tests were carried out by using two different apparatuses:

1) The simultaneous thermal analysis (STA) which consists of differential calorimetric analysis and thermogravimetry was carried out in a thermal analyzer Linseis STA PT-1000 (Germany). The flow of N_2 gas was 20 mL/min, heating rate of – 10°C/min; the temperature ranged from RT up to 1000°C. Ceramic sample handlers and PT/10%Rh crucibles were used.

2) Differential scanning calorimetry (DSC) and specific heat measurement was carried using Netzsch DSC 214 Polyma (Germany). The heating rate was 5°C/min, the temperature ranged from 10°C up to 50°C; the flow of N_2 gas was 20 mL/min. Ceramic sample handlers and Al crucibles were used.

Fourier transform infrared spectroscopy (FTIR) analysis. Fourier transform infrared spectroscopy (FTIR) spectra were carried out with the spectrometer Perkin Elmer FT-IR system Spectrum X (USA). The specimens were prepared by mixing 1 mg of the sample material in 200 mg of KBr. Spectral analysis was performed in the range of 4000–400 cm^{-1} with the spectral resolution of 1 cm^{-1}.

Determination of specific surface area. The specific surface area was determined by Brunauer, Emmet, and Taller (BET) method. The measurements were performed on Autosorb iQ (Quantachrome Instruments, JAV). Sorptometer (Costech Instruments, USA) using a nitrogen adsorption isotherm 77 K. The specific surface area was calculated according to the BET equation, using N_2 adsorption isotherm data in the range of $0.05 < P/P_0 < 0.35$.

The mineralogical composition of the hydration products was as follows: OPC with 7.5 wt.%. Different additives (CA1 – (350°C), CA2 – (550°C), CA3 – (900°C)) were formed when the water/cementitious mixtures ratio was 0.5 at 25°C. The hydration process was stopped with ethanol. Finally, the products were crushed and dried at 50°C temperature for 24 h.

The heat evolution rate of the manufactured binder during the hydration was investigated by using an eight-channel isothermal calorimeter TAM Air III (TA Instruments). Glass ampoules (20 ml), each containing 3 g of the dry material, were placed in the calorimeter and the injection units for each ampoule filled with 1.5 g of water. Having reached the isothermal conditions (25±0.1°C), the water was injected into the ampoules and mixed inside the calorimeter with the dry material for 20 s (frequency 2–3 s^{-1}). The heat evolution rate was measured over a period of 72 h.

Adsorption experiments were carried out at 25°C in the thermostatic adsorber Grant SUB14 for different time periods (3, 20 and 60 min). 1 g of adsorbent (CA1; CA2 or CA3) was added to 100 ml of $CuSO_4$ aqueous solution containing 0.5, 1, 3, and 5 g/l of Cu^{2+} ions. The amount of the adsorbed (Cu^{2+}) and (SO_4^{2-}) ions was determined on the basis of the changes of the concentration of cations in the solution at different durations (3, 20, and 60 min). The concentrations of Cu^{2+} and SO_4^{2-} ions were determined by the colorimetric method (Colorimeter DR890, Hach Lange).

The thermal stability of samples was investigated in a furnace Nabertherm LH 15/13 within the 350–950°C temperature range for 1 h when the heating rate was equal to 6°C/min.

The microstructure of the materials was observed by using **scanning electron microscopy (SEM)** (Model JSM-7600F, JEOL Co., Japan) coupled with **energy dispersive X-ray spectrometry (EDX)** (Inca Energy 350, Oxford Instruments, Silicon Drift type detector X-Max20) performed by using accelerated voltage of 10kV, the 32 working distance of 8.6 and 8.7 mm for SEM observation, and 200 s accumulation time for EDX analysis. The samples were affixed to the SEM specimen holder by using epoxy resin and then sputter-coated with gold aimed to promote electrical conductivity.
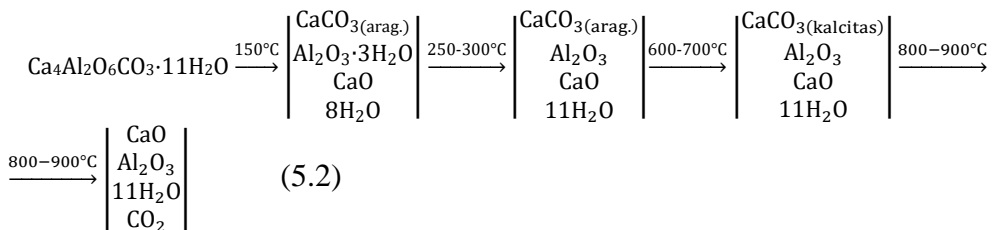
5.3 RESULTS AND THEIR DISCUSSION

5.3.1. Formed compounds in the CaO−Al₂O₃−H₂O system and their thermal properties when the C/A ratio is equal to 1.7

It was determined that in unstirred CaO–Al_2O_3–H_2O suspensions when CaO/Al_2O_3 molar ratio of primary mixture was equal to 1.714, within 1 h of isothermal curing at 130°C calcium monocarboaluminate—$Ca_4Al_2O_6CO_3 \cdot 11H_2O$ and

hydrogarnet–katoite ($Ca_3Al_2(OH)_{12}$) were formed (Fig. 5.1, a, curve 1). Also, the basic reflections of partially unreacted gibbsite ($Al(OH)_3$) and the traces of calcium carbonate ($CaCO_3$;) were observed in X-ray diffraction patterns (Fig. 5.1, a, curve 1).

Fig. 5.1 XRD patterns (a) and DSC curves (b) of synthesis products in the mixtures with C/A molar ratio of 1.714, when the duration of hydrothermal treatment at 130°C temperature is h: 1—1; 2—4; 3—16; and 4—72. Indices: c—calcium monocarboaluminate ($Ca_4Al_2O_6CO_3 \cdot 11H_2O$); k—katoite ($Ca_3Al_2(OH)_{12}$); g—gibbsite ($Al(OH)_3$); d—calcite ($CaCO_3$); and b—boehmite ($AlO(OH)$)

After 4 h of hydrothermal treatment, XRD analysis data showed that only the basic diffraction maximum intensity of $Ca_4Al_2O_6CO_3 \cdot 11H_2O$ significantly increases (Fig. 5.1, curve 2). In comparison with the products obtained after 1 h of synthesis, it was observed that the other compounds remained stable (Fig. 5.1, a, curve 1–2). It was determined that after 16 h of hydrothermal treatment, calcium monocarboaluminate decomposed to $CaCO_3$ and $Ca_3Al_2(OH)_{12}$, because the intensity of diffraction maximums characteristics to calcite and katoite increased (Fig. 5.1, a, curve 3). The obtained results were confirmed by STA analysis data (Fig. 5.1, b). On the DSC curve, at 150°C temperature, the broad endothermic peak is characteristic to the decomposition of calcium monocarboaluminate (first endothermic effect). It was observed that after 1–4 h of synthesis, the heat of this endothermic effect increased from 98.06 to 110.77 J/g (Fig. 5.1, b, curve 1–2). By prolonging the duration of synthesis to 24 or 72 h, the formation of mentioned compound is inhibited and the heat values were two times lower (Fig. 5.1, b, curve 3–4).

11

It should be noted that the decomposition of gibbsite (second endothermic effect) as well as the decomposition of katoite (third endothermic effect) overlapped in a 240–320°C temperature range. It is clearly visible that the third endothermic peak characteristic to the decomposition of katoite almost does not change even after continuing the synthesis to 72 h. Meanwhile, the area of the second endothermic peak decreased, when the duration of synthesis was extended and after 72 h, it is completely separated. Meanwhile, within 16–72 h of hydrothermal treatment, STA analysis data showed that at 460°C the amount of adsorbed heat attributed to dehydration of boehmite (fourth endothermic effect) was increased from 39.07 to 121.04 J/g (Fig. 5.1, b). It was also supported by XRD results, which indicated that gibbsite recrystallized to boehmite.

In order to evaluate the thermal behavior of primary synthesis products, the products were calcined by performing in situ XRD. The synthesis product, which was obtained after 4 h of hydrothermal treatment at 130°C temperature, was examined in a high-temperature camera MTC-hightemp in a 25–1150°C temperature range. It was estimated that calcium monocarboaluminate is stable till 125°C, because the diffraction maximums characteristic to the mentioned compound remain unchanged. Meanwhile, at a higher temperature (125–150°C), the latter compound fully decomposed. Furthermore, when the temperature of calcination was increased to 300°C, gibbsite was fully dehydroxylated. Meanwhile, at 350°C, the crystalline structure of katoite was destroyed and the mentioned compound recrystallized to mayenite. After this process, when intensive diffraction peaks characteristic to katoite disappeared, the reflections of aragonite (d-spacing–0.3397, 0.3274 nm) became visible. It was examined that when the temperature of calcination was increased to 600°C, aragonite became metastable and recrystallized to calcite. It is worth mentioning that when the calcination temperature varied in a 850–1150°C range, the intensity of diffraction maximums, which are characteristic to mayenite, increased. Furthermore, calcite fully decomposed to calcium oxide at 900°C. It is possible to assume that during experiments of the calcination of calcium monocarboaluminate, the phase transformation occurred in the following sequence:

$$
Ca_4Al_2O_6CO_3 \cdot 11H_2O \xrightarrow{150°C} \begin{vmatrix} CaCO_{3(arag.)} \\ Al_2O_3 \cdot 3H_2O \\ CaO \\ 8H_2O \end{vmatrix} \xrightarrow{250\text{-}300°C} \begin{vmatrix} CaCO_{3(arag.)} \\ Al_2O_3 \\ CaO \\ 11H_2O \end{vmatrix} \xrightarrow{600\text{-}700°C} \begin{vmatrix} CaCO_{3(kalcitas)} \\ Al_2O_3 \\ CaO \\ 11H_2O \end{vmatrix} \xrightarrow{800-900°C}
$$

$$
\xrightarrow{800-900°C} \begin{vmatrix} CaO \\ Al_2O_3 \\ 11H_2O \\ CO_2 \end{vmatrix} \qquad (5.2)
$$

5.3.2. Formed compounds in the CaO−Al₂O₃−H₂O system and their thermal properties when the C/A ratio is equal 2.8−3.2

It was found that in the CaO–Al₂O₃–H₂O system, within 4 h of isothermal treatment at 130°C, calcium aluminum hydrate katoite (Ca₃Al₂(OH)₁₂) was formed. The best synthesis results are observed after the 4 h hydrothermal treatment with 2.8,

meanwhile, with a longer duration of the hydrothermal reaction (72 h), in addition to the target synthesis product, calcium monocarboaluminate, boehmite, and portlandite were also identified (Fig. 5.2, a). After determining the optimal C/A ratio, the next stage of research analyzes the influence of the duration of hydrothermal treatment on the formation of katoite. It was determined that katoite was formed (Fig 5.2, b). Also, typical reflections of partially unreacted portlandite were observed in the XRD pattern. The partial carbonization of the synthesis products and/or unreacted primary components was observed when they were dried in an air-conditioned chamber because the diffraction maximum typical to calcium monocarboaluminate was determined (Fig. 5.2, b, pattern 1). It was determined that after 4 h of isothermal curing, only traces of portlandite and intensive diffraction peaks characteristic to $Ca_3Al_2(OH)_{12}$ were detected in the synthesis products (Fig. 2, b pattern 2).
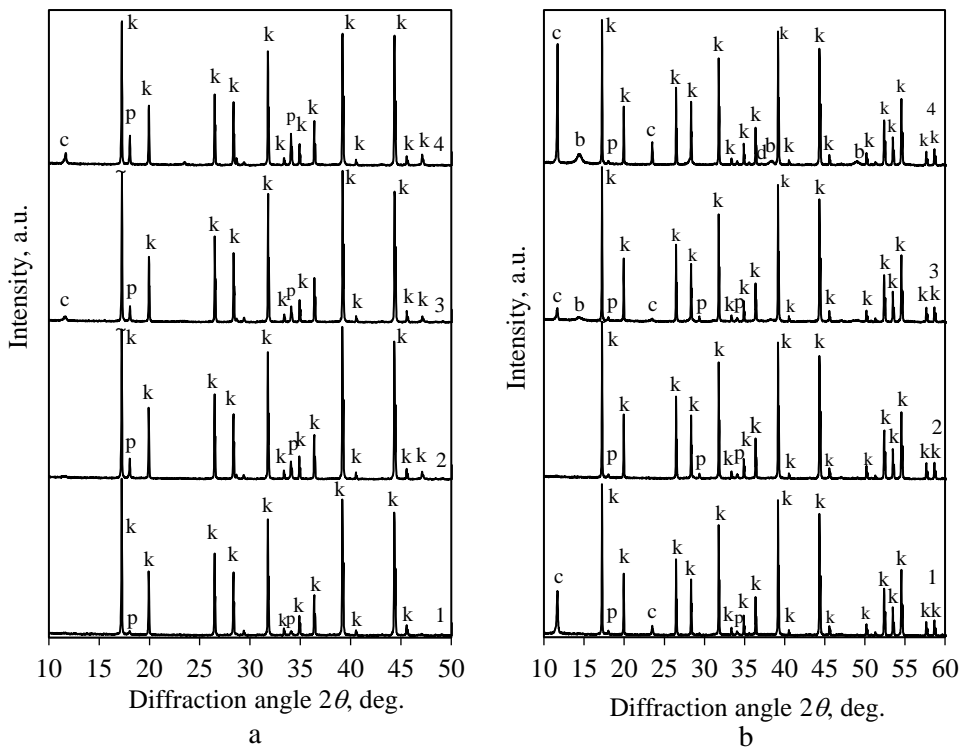
Fig. 5.2. XRD curves of synthesis products in the mixtures with C/A molar ratio range 2.8–3.2: 1–2.8, 2–2.9, 3–3, 4–3.2 (a), and XRD curves of synthesis products in the mixtures with C/A molar ratio 2.8 when the duration of hydrothermal treatment is, h: 1–1h; 2–4h; 3–16h; 4–24h; 5–72h. Indexes: c – calcium monocarboaluminate; k – katoite; b – boehmite; p – portlandite.

It should be noted that after 16–72 h of hydrothermal treatment, katoite started decomposing because the intensity of the diffraction peaks characteristic to this compound slightly decreased and the typical diffraction maximums characteristic to calcium monocarboaluminate and boehmite were observed (Fig. 5.2, patterns 3–4).

13

The obtained results showed that a higher quantity of pure katoite formed after 4 h of isothermal curing. For this reason, this synthesis product was characterized by thermal analysis.
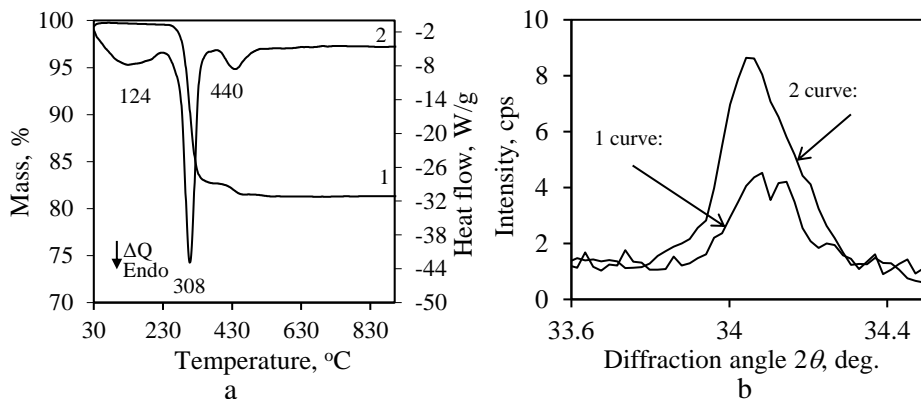
Fig. 5.3 STA curves of synthesis products after 4 h of hydrothermal treatment (a: 1 – TGA; 2 – DSC) and the change of the main diffraction peaks of portlandite (b): after 4 h of hydrothermal duration (pattern 1) and after 1 h of treatment at 350°C (pattern 2).

The typical thermal behavior of the formed crystalline compounds was determined in the STA curves. In the DSC curve, the broad endothermic effect in 30–230°C temperature range can be assigned to the removal of adsorbed water from the synthetic products. The decomposition of katoite was observed at 240–380°C temperature. The final endothermic effect within the temperature interval of 400–500°C is related to the decomposition of portlandite. TGA data showed that during dehydration of portlandite, the mass loss is 1.25%, which is equal to 5.13% of portlandite (Fig. 5.3, a). This value was calculated with equation $W_{portlandite} = M_{Portlandite}$ (74 g/mol)/(M_{water}(18 g/mol) · TGA (1.25%). It should be noted that at the process of partial katoite dehydration (at 308°C), the extra/additional portlandite was formed which decomposed at the same time with the primary portlandite at ~440°C temperature. For this reason, more information was obtained from QXRD analysis: the determined results showed that after thermal treatment at 350°C temperature, the main diffraction peak area of portlandite increased ~5 times (Fig. 5.3, b). It was calculated that the quantity of portlandite increased from 1.00% (in the sample before calcination) to 5.47% (in the sample after calcination at 350°C) (Fig. 5.3, b).

In order to evaluate the thermal behavior of primary synthesis products, in the next stage of this work the products were calcined by performing in-situ XRD. The results of in-situ XRD analysis showed that katoite is stable up to 275°C because the reflections typical to that compound remained stable (Fig. 5.4). At a higher temperature (350°C), katoite fully transformed into mayenite, and the basic diffraction peak of portlandite (d-spacing – 0.2620 nm) increased. The obtained results show that at 450°C temperature portlandite fully dehydrated into CaO, and the crystallinity of mayenite decreased by increasing the temperature to 750°C. In addition, when the temperature was increased (750°C–1150°C), the diffraction peaks typical to mayenite and CaO also increased.
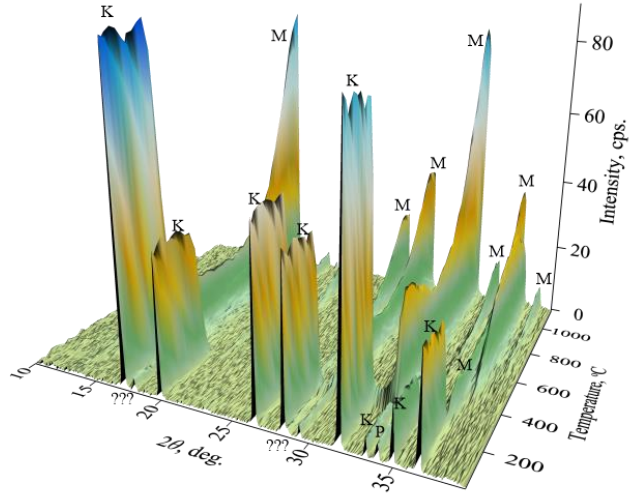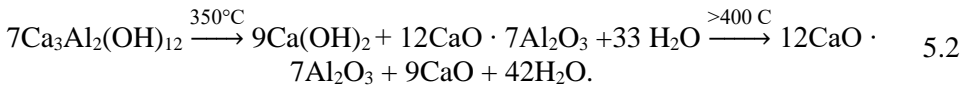
14

Fig. 5.4 XRD patterns (in-situ) of the synthesis product (hydrothermal duration 4 h at 130°C temperature) after thermal treatment from 25 to 1150°C. Indexes: k – katoite; p – portlandite; M − mayenite; L – CaO.

It is possible that katoite decomposed to mayenite and lower crystallinity CaO mixture because the decomposition of C_3AH_6 most likely occurs according to reaction:

$$7Ca_3Al_2(OH)_{12} \xrightarrow{350°C} 9Ca(OH)_2 + 12CaO \cdot 7Al_2O_3 + 33 H_2O \xrightarrow{>400 C} 12CaO \cdot 7Al_2O_3 + 9CaO + 42H_2O. \qquad 5.2$$

Another important physical parameter that directly determines the possibilities of using products is the specific surface area. It was obtained that a stable monolayer of absorbed N_2 was formed on the surface of all samples, because straight lines were obtained for all samples in a BET coordination ($0.05 \leq p/p0 \leq 0.30$) and correlation coefficients R^2 remained very close to the unit, i.e. 0.998 (Fig.5.5). In addition, the calculated C_{BET} constant values varied in the range from 50 to 250 in all conditions. This fact confirmed that the calculated S_{BET} value is correct because only one adsorption layer of nitrogen in 0.05–0.35 p/p_0 range were formed. It was noted that the specific surface area (S_{BET}) was equal to 9.23 m^2/g of synthetic katoite. The obtained data showed that the specific surface area of mayenite depends on calcination temperature. It was determined that S_{BET} of mayenite was equal to 11.11 m^2/g after calcination at 350°C temperature. Meanwhile, at a higher temperature (550°C), the value of S_{BET} slightly decreased to 9.98 m^2/g. It should be noted that S_{BET} value characteristic for calcination product increased more than two times to 24.55 m^2/g after calcination at 900°C. In all samples, nitrogen adsorption and desorption isotherms formed hysteresis loops. The hysteresis loops of pure katoite and calcined katoite at 350°C; 550°C temperature samples are not suitable for either type of IUPAC classifications. It should be emphasized that the mentioned samples form is typical as

H3 type, but the adsorption and desorption isotherms must coincide in the range of relative pressures p/p0 ≈ 0.30. Meanwhile, in our case these isotherms intersected when relative pressure p/p0 = 0.70–0.8, which is characteristic for H1 type loops. The calculation revealed that the hysteresis loops of mayenite prepared at 900°C temperature is of H1 type, which is characteristic for materials with well-defined cylindrical-like pore agglomerates (Fig. 5.5 b).
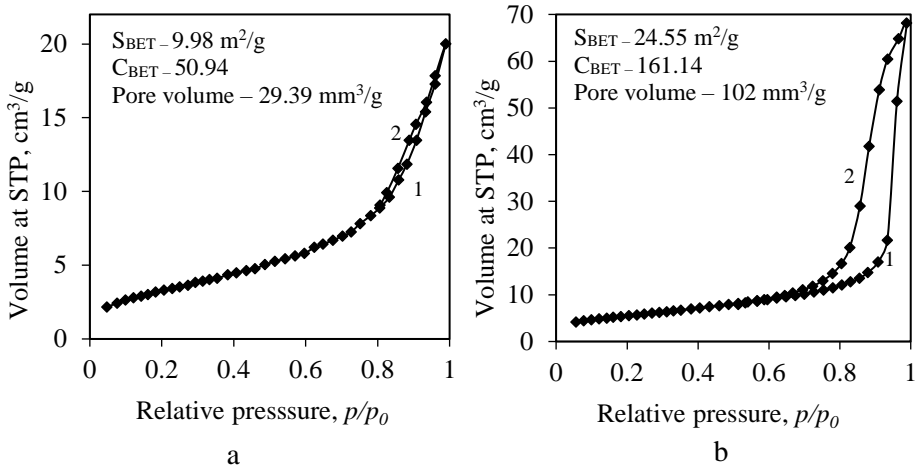

Fig. 5.5. Adsorption (1) – desorption (2) isotherms of calcined products for 1 h at a different calcination temperature, °C: a – 550°C, b – 900°C.

It was determined that the total pore volume of pure katoite and formed mayenite at 350–550°C temperature samples was equal to ~30 mm^3/g and it increased more than 3 times after calcination at 900°C. It is likely that at a higher calcination temperature (900°C), the formation of new pores proceeded, which led to an increased total pore volume.

5.3.3. Influence of synthetic mayenite derivatives on early hydration of Portland cement

In the next stage, the influence of a calcined additive with a different mineral composition on the hydration of cement samples was determined: CA1 – (350°C), CA2 – (550°C), CA3 – (900°C) additive (2.5, 5 and 7.5 wt%) were replacement part of OPC. The heat release kinetics were calculated based on pure OPC weight: real measured values (Q_{real},W/g) were recalculated to present values ($Q_{presented}$,W/g)= (Q_{real},W/g)/(OPC in parts per unit mass; 0.975; 0.95; 0.925). After 72 h of hydration, the highest quantity of the total heat (300–350 J/g) was obtained in the mixtures with 7.5% of CA, while, in the samples with 5% of additives, it reached only 268–292 J/g, which was slightly higher than the value obtained in the pure OPC sample (~248 J/g) (Table 2). Therefore, the mixtures with 7.5% of CA were further investigated in detail. Synthetic calcined additives accelerated the first reaction (1–3 min) of cement samples because the maximum heat evolution rate increased from 0.005 W/g (pure OPC) to 0.1 W/g (OPC with additives (7.5%)).

16

Table 5.1. Heat of cement paste with synthetic calcined additive

Additive, %	Sample	Calcinated temperature, °C	Duration of hydration, h						
			0.3	1	3	10	15	24	72
			Total heat after, J/g						
Pure OPC			3.5	6.3	10	53.9	97.3	157	248
7.5	OPC-7,5-CA1	350	58	76	85	128	160	201	300
	OPC-7,5-CA2	550	44	100	112	165	201	248	336
	OPC-7,5-CA3	900	83	98	110	157	195	249	350

Moreover, the new exothermic reaction was identified in the cases of OPC-7,5-CA2 and OPC-7,5-CA3. In addition, the induction period was shortened to approximately 2.2 h for OPC-7,5-CA1, while it lasted 3 h for pure OPC. Meanwhile, the lowest peak of reaction II: tricalcium silicate hydration was determined in OPC samples with additives. In addition, reaction III, typical of calcium aluminate hydration and ettringite formation, was not identified in the OPC samples with additives (Fig. 5.6).
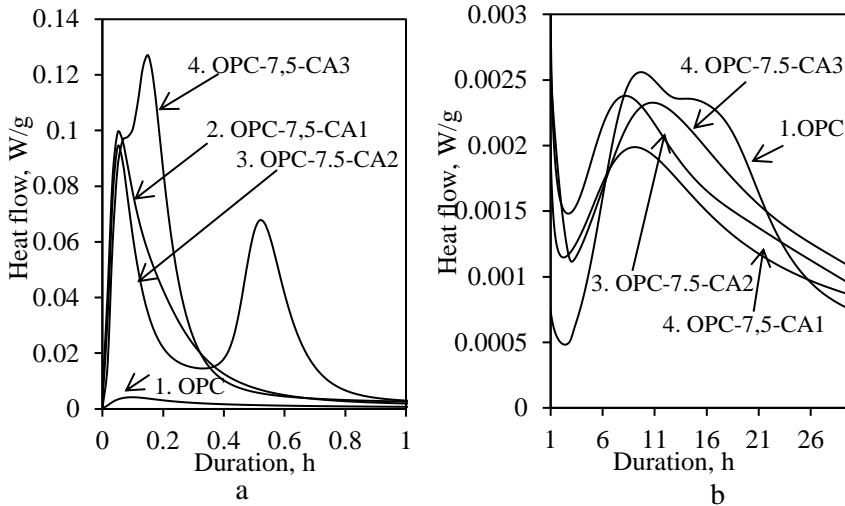
Fig. 5.6. Heat flow of OPC, OPC-CA1, OPC-CA2 and OPC-CA3 curves during hydration process.

It was established that the interaction of gypsum and the formation of ettringite depends on the reactivity of the additive, and the proceeding reaction can be written as:

$$C_{12}A_7 + 12C\hat{S}H_2 + 137H \rightarrow 4C_6A\hat{S}_3H_{32} + 3AH_3(gel) \tag{5.3}$$

This first reaction was confirmed by STA results: at ~86°C, the amount of the absorbed heat typical to the dehydration of AH_3 gel was observed in the OPC samples

17

with the additives. It was determined that the calcination temperature of additives exerts significant influence on the hydration rate of mayenite with gypsum. Thus, the obtained results indicate that at the first stage (after 3 min) of hydration, the calcination temperature exerts negative influence on the formation of ettringite, although it also slows down the intensity of the main diffraction peak of the gypsum. However, during the following hydration step (3–21 min), the reaction of the gypsum with the calcined additive at 900°C is more accelerated as well as the formation of ettringite in view of the reduction or increased peak intensities related to these compounds (5.2 table).

Table 5.2. Intensity changes of gypsum ettringite and mayenite main diffraction peak in samples during hydration process.

Compounds	Sample	Intensity of the main diffraction peak			
Hydration duration, min		0	3	21	60
Gypsum	OPC	70.83	52.53	43.57	41.2
	OPC-7.5-CA1	65.42	3.7	2.03	0
	OPC-7.5-CA2	70.36	11.67	0.5	0
	OPC-7.5-CA3	70.31	19.76	3.85	0
Ettringite	OPC	0	0.65	0.78	2.37
	OPC-7.5-CA1	0	3.57	3.41	2.89
	OPC-7.5-CA2	0	3.78	3.75	2.24
	OPC-7.5-CA3	0	2.97	4.71	3.6
Mayenite	OPC-7.5-CA1	2.66	2.58	1.34	0
	OPC-7.5-CA2	3.65	3.39	1.67	0
	OPC-7.5-CA3	5.03	4.43	2.12	0

When hydration is extended to more than 1 h, the gypsum reaction is completed because the diffraction maximums typical of this compound are not detected in any sample with additives. On the other hand, there is insignificant decrease in the intensity of the ettringite diffraction maximums. However, in the pure system, it was determined that the gypsum reaction and ettringite formation are directly dependent on the duration of hydration (5.2 table). The fact that unreacted mayenite is still present in all the samples after 21 min hydration was confirmed by XRD analysis. The obtained results show that after 21 min of hydration, the main diffraction maximum typical of mayenite decreases by ~55% in comparison with the samples before hydration (5.2 table). It was established that during the next stage of hydration (21–60 min), the used additives stimulate the formation of CASH or/and monosulphate or/and CAH because a broad basal reflection typical of the above-mentioned compounds was identified in the interval of 9–13 diffraction angles (Fig. 5.7).
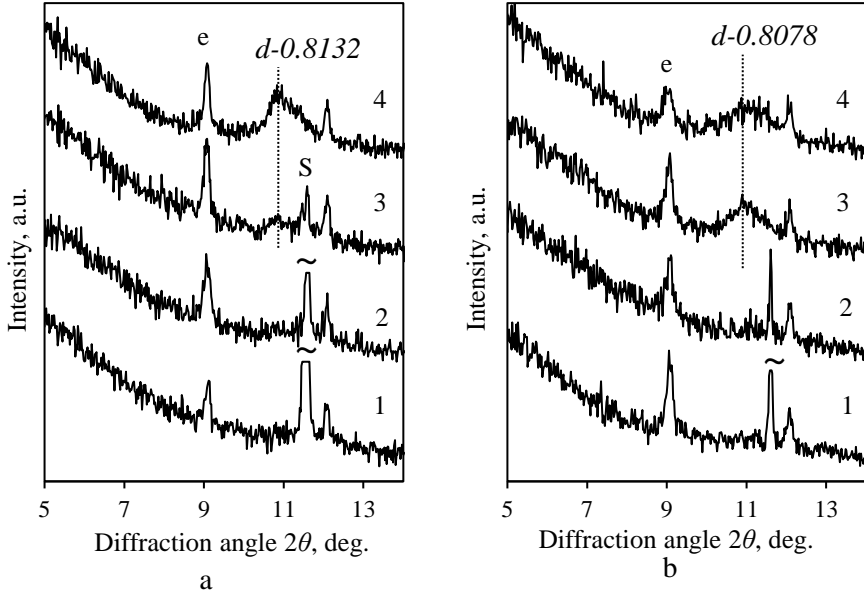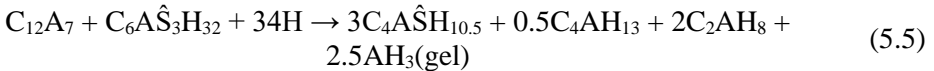
Fig. 5.7. XRD patterns of OPC-CA2 (a) and OPC-CA3 (b) samples after different hydration times, h: 1–3 min; 1.5–9 min; 2–21 min; 3–32 min; 4–60 min. Indexes: e− ettringite, g–gypsum.

The mechanism of hydration (21–60 min) depends mostly on the calcination temperature of mayenite. The sequential reactions in the systems OPC-CA1 and OPC-CA3 at this stage of hydration could be described by the following routes: during this period, ettringite is partially decomposed into monosulfoaluminate and gypsum according to Eq (5.4):

$$C_6A\hat{S}_3H_{32} \leftrightarrow C_4A\hat{S}H_{10.5} + 2C\hat{S}H_2 + 16H \qquad (5.4)$$
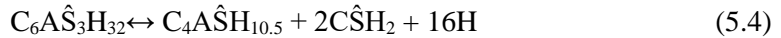
After this period, part of unreacted mayenite and the newly formed gypsum (Eq. 5.4) were found to be still present in all the samples. Therefore, these components can again react to form new or secondary ettringite (Eq. 5.3). It was observed that the intensity of the diffraction peak characteristics to ettringite insignificantly decreased, and gypsum fully disappeared in the samples after 60 min of hydration (5.2 table). Meanwhile, in the OPC-CA2 system, the mechanism of hydration is different. The new exothermic reaction can be described by the following equation:

$$C_{12}A_7 + C_6A\hat{S}_3H_{32} + 34H \rightarrow 3C_4A\hat{S}H_{10.5} + 0.5C_4AH_{13} + 2C_2AH_8 + \qquad (5.5)$$
$$2.5AH_3(gel)$$

This highly simplified reaction equation shows only the direction of this process. It was determined that after 60 min of hydration, a new broad basal reflection (d-0.8078 nm; 2θ–10.89 deg.) was formed in the sample (Fig. 5.7a). This broad basal reflection shifts to the range of higher diffraction angles and can be assigned to monosulfoaluminate and semi-crystalline structure (hydroxy-AFm) compounds

which partially overlap. Also, this reaction (Eq. 5.5) was confirmed by a significantly decreasing diffraction peak which is characteristic to ettringite (Table 5.2).

5.3.4. Tailoring of mayenite derivatives for adsorption of Cu^{2+} and SO_4^{2-} ions

Heavy metals are not only some of the most difficult pollutants to clean up, they also have a negative impact on the environment. Anions (such as sulphate, nitrate, phosphate, etc.) are slightly less harmful, but their solubility in water is much higher. Increasing industrial development has highlighted today's wastewater treatment problems and the need to develop efficient, low-cost, and environmentally friendly materials that effectively remove both cationic and anionic pollutants simultaneously. The results discussed in the previous section are also quite optimistic, as a high chemical activity of synthetic mayenite derivatives is observed at the beginning of hydration. It was therefore decided to determine the adsorption capacity of synthetic mayenite derivatives for both cations and anions simultaneously. One of the most widely used heavy metals in the industry and subsequently detected in wastewater, copper, and one of the more difficult cations to treat, SO_4^{2-}, which is also highly abundant in industrial wastewater, were chosen for this study. After the adsorption process, the mayenite with the harmful Cu^{2+} and SO_4^{2-} ions present can be recovered in the cement stone, which will help to address the risk of secondary pollution.

5.3.4.1 Adsorption capacity of mayenite derivatives for Cu^{2+} and SO_4^{2-} ions in 500 mg/l copper sulphate solution and thermal stability of obtained products

The experiment of Cu^{2+} ion adsorption by using samples calcined at 350°C (CA1) and 900°C (CA3) temperature, which differ in structural properties (specific surface area), was investigated. It was determined that the calcination temperature of products greatly affected their adsorption capacity for cooper ions. It was observed that after 3 min of adsorption more than 94% of cooper ions were already intercalated into the structure of mayenite, i.e. ~47 mg Cu^{2+}/g, when the initial solution concentration was equal to 500 mg/l. The adsorption process ended after 60 min, when almost all cooper ions were intercalated (~99%). It should be mentioned that mayenite also adsorbed SO_4^{2-} anions, because they did not appear in the aqueous solution after 60 min under all experimental conditions. Besides, the largest amount of Cu^{2+} ions was adsorbed when mayenite formed at 900°C temperature was used.
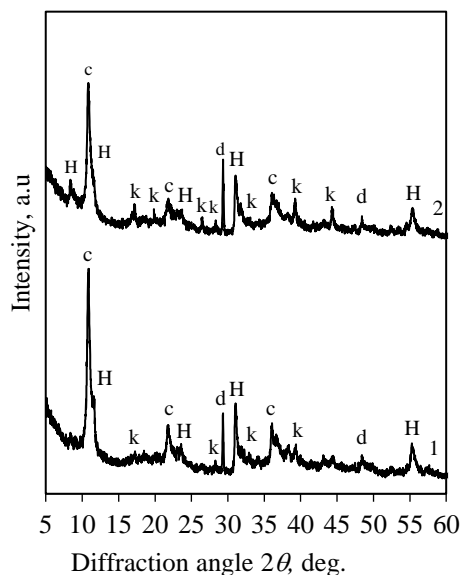
Fig. 5.8. XRD patterns of products after adsorption processes (curve 1 – when using calcined at 350°C (CA1); curve 2 – when using calcined at 900°C (CA3)). Indexes: c – calcium aluminium carbonate hydroxide hydrate; d– calcite; k –katoite; H – LDH group compounds.

It was determined that after the mentioned process in the sample prepared at 350°C (CA1), calcium monocarboaluminate ($Ca_4Al_2O_6CO_3 \cdot 11H_2O$), calcite and traces of katoite were formed (Fig. 5.8, curve 1). Also, new hydrotalcite group compounds were observed in X-ray diffraction patterns. This can be explained by the fact that no other compounds which consist of Cu^{2+} and SO_4^{2-} ions were identified in XRD patterns. Thus, all mentioned ions were bound to form new layered double hydroxides (LDH). Meanwhile, when the mayenite was prepared at 900°C temperature (CA3), XRD analysis data showed that the diffraction maximum intensity of katoite and LDH insignificantly increased (Fig. 5.8, curve 2).

The thermal stability of the products after adsorption processes (when using adsorbent calcined at 900°C) was investigated in a high-temperature camera MTC-hightemp in a 25–1000°C temperature range (Fig. 8). It was estimated that calcium monocarboaluminate and LDH is stable up to 175°C, whereas at a higher temperature (175–200°C), the latter compounds fully decomposed. The results demonstrate that the intensities of diffraction peaks characteristic for katoite were almost the same with increasing calcination temperature (from 25°C to 275°C).
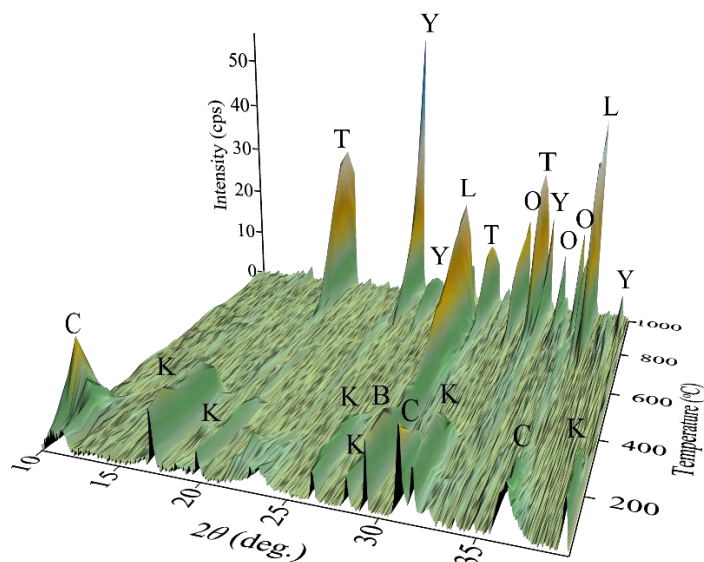
Fig. 5.9. In situ XRD patterns of the products after adsorption processes (when using adsorbent calcined at 900°C), when the temperature of calcination is 25–1000°C. Indices: K – katoite; C – calcium monocarboaluminate; O – calcium copper oxide (Ca_2CuO_3); Y – ye'elimite; T – tricalcium aluminate; L – lime.

Meanwhile, at a higher temperature (350°C), katoite fully destroyed to amorphous structure compounds. It was determined that the calcite fully decomposed to calcium oxide at 700°C. It should be underlined that when the temperature of calcinations was increased to 800°C, amorphous structure compounds started recrystallizing to ye'elimite, tricalcium aluminate, and calcium copper oxide. It was determined that the crystallinity of mentioned compounds increased by increasing the temperature to 1000°C.

5.3.4.2. Adsorption capacity of mayenite derivatives for Cu^{2+}/SO_4^{2-} ions, influence of copper ion concentration on adsorption processes, and secondary adsorbent use

It was determined that the calcination temperature of mayenite (CA1 – (350°C), CA2 – (550°C), CA3 – (900°C)) affected their adsorption capacity for copper ions and SO_4^{2-} anions. It was obtained that after 3 min of adsorption in a solution containing 1 g/l of copper ions, the amount of the adsorbed ions by CA1 was equal to 39 mg Cu^{2+}/l (39%). Meanwhile, after 60 min, all Cu^{2+} ions (100 mg/g) were adsorbed, and 58% of SO_4^{2-} anions were intercalated into the structure of mayenite (CA1), i.e., ~87 mg SO_4^{2-}/g. It is worth noting that the Cu^{2+} and SO_4^{2-} adsorption capacity of mayenite (CA1) decreased by increasing the initial concentration of copper ions in the solution to 3 g/l because after 60 min of this process, the determined values were equal to 50 mg of Cu^{2+} ions and 80 mg of SO_4^{2-} anions, respectively. A further increment of the initial concentration of copper ions (5 g/l) had a negative effect on the total adsorbed ions.

Table 5.3 The amount of adsorbed Cu^{2+} ions and SO_4^{2-} anions, under different conditions

The primary aqueas solution containing g/l of Cu^{2+} ions		1 g/l pH = 4.87		3 g/l pH=4.00		5 g/l pH = 3.85	
Sample	Duration of adsorption, min	The amount of adsorbed Cu^{2+} ions and SO_4^{2-} anions, mg/g					
		Cu^{2+}	SO_4^{2-}	Cu^{2+}	SO_4^{2-}	Cu^{2+}	SO_4^{2-}
CA1	3	39	40	42	45	23	40
	20	100	75	42	55	33	50
	60	100	87	50	80	38	60
pH value after adsorption		9.65		5.15		4.89	
CA2	3	29	35	14	70	18	50
	20	70	65	32	65	26	70
	60	81	82	46	80	59	85
pH value after adsorption		8.12		5.04		4.72	
CA3	3	27	20	28	34	57	80
	20	73	61	41	48	58	90
	60	77	80	63	82	93	98
pH value after adsorption		10.48		5.14		4.97	

It was observed that the calcination temperature of the products exerts negative influence on the adsorption capacity of Cu^{2+} ions and SO_4^{2-} anions when the initial concentration of copper ions is equal to 1 g/l. It should be emphasized that within 20 min of copper ions adsorption (when the sample was synthesized at 550–900°C (CA2 and CA3), the adsorbed amount of the above-mentioned ions increased to 27–29 mg/g, and after 1 h, it was equal to 77–81 mg/g. Meanwhile, in the case of SO_4^{2-} anions adsorption by the above-mentioned samples, the removal efficiency was insignificantly lower, and the maximum amount of the adsorbed anions (80–82 mg/g) was obtained after 60 min. It was determined that the adsorption capacity of CA2 and CA3 mayenite samples decreased by increasing the initial concentration of copper ions in the solution to 3 g/l. It can be assumed that the largest total capacity of mayenite synthesized at 900°C temperature (CA3) is ~63 mg Cu^{2+}/g. It was observed that the SO_4^{2-} anions adsorption capacity of CA2 and CA3 mayenite samples was still the same when increasing the initial concentration of copper ions (3 g/l) because, after 60 min of adsorption, 80–82 mg of SO_4^{2-} anions was adsorbed by 1 g of CA2 or CA3 samples. When the concentration of copper ions in the solution was increased to 5 g/dm³, the adsorption capacity of CA2 and CA3 mayenite samples insignificantly increased. Thus, the largest amount of Cu^{2+} ions was adsorbed by CA1 mayenite sample (100 mg/g) when the initial concentration of copper ions in the solution to 1 g/l and the total SO_4^{2-} ions adsorption capacity of the above-mentioned sample is

slightly lower (87 mg/g) than in CA3 sample from the higher concentration copper solutions. It should be noted that S_{BET} and the total pore volume values of mayenite, which in CA1 and CA3 samples increased by 2 and 3 times, respectively, did not affect the adsorption capacity of Cu^{2+}/SO_4^{2-} ions. Presumably, low solubility portlandite (1.13 gCaO/1000 gH_2O) had a positive effect on the CA1 adsorbent adsorption capacity. However, if we calculated the total adsorption capacity of both ions (the total quantity of Cu^{2+} and SO_4^{2-} ions, i.e., ~187 mg/g) of CA1 adsorbent, we would have very close values.

It was detected that mayenite is not stable during the adsorption process, and it fully reacted under all experimental conditions. After the adsorption process in the solution with a lower concertation of copper ions, katoite (PDF No. 024–0217; d – 5.130; 4.442; 3.358 nm), ettringite (PDF No. 013–3691; d – 9.725; 5.614; 3.881 nm), and products of partial carbonization – calcium aluminium carbonate hydroxide hydrate ($Ca_2Al(CO_3)_{0.25}(OH)_{6.5}(H_2O)_2$; PDF No. 018–9908; d – 8.135; 4.068; 2.888 nm); calcium aluminium carbonate hydroxide hydrate ($Ca_4Al_2(CO_3)OH_{12}(H_2O)_5$; PDF No. 011–4223; d – 7.554; 3.777; 3.809 nm); and calcite (PDF No. 001–0837; d – 3.04; 1.92; 1.87 nm)) were determined in all adsorbent samples. Meanwhile, after adsorption in the solution with a higher concentration of copper ions (3 g/l and 5 g/l), the diffraction peaks characteristic to katoite decreased when increasing the concentration of copper ions in the initial solution. Presumably, the stability of katoite at low pH values decreased when increasing the concentration of copper ions. It is worth noting that under these conditions, a compound containing copper ions – copper sulphate hydroxide hydrate – posnjakite ($Cu_4SO_4(OH)_6H_2O$; PDF No. 010–7185; d – 6.944; 3.472; 2.423 nm) – was formed (fig. 5.10, a).
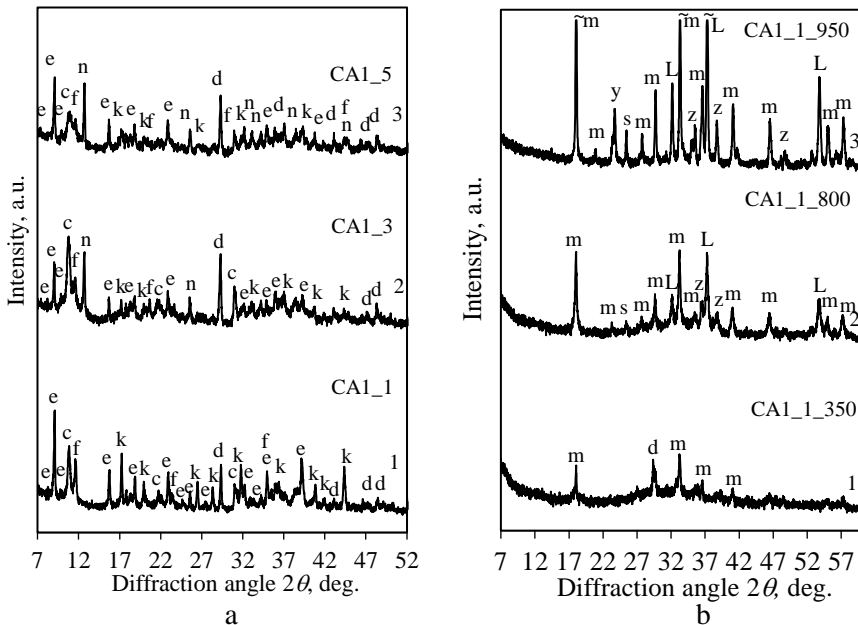
Fig. 5.10. XRD (a) curve 1 – 1 g/l $CuSO_4$; curve 2 – 3 g/l $CuSO_4$; curve 3 – 5 g/l $CuSO_4$, and XRD patterns of products after the first adsorption processes (1 g/l $CuSO_4$) and calcination (curve 1 – 350°C, curve 2 – 800°C, curve 3 – 950°C) when using adsorbent CA1. Indexes: e − ettringite, c – calcium aluminium carbonate hydroxide hydrate, k – katoite, d – calcite, f – calcium aluminium carbonate hydroxide hydrate, n – posnjakite, Y – ye'elimite, L – lime, d – calcite, m – mayenite, s – calcium sulfate, z – CuO.

The thermal stability of the products after adsorption processes when the initial solution concentration of Cu^{2+} ions was equal to 1 g/l, was investigated within the 350–950°C temperature range (Fig 5.10, b). It was determined that at 350°C, katoite was fully destroyed to mayenite, and the crystal structures of ettringite, calcium aluminium carbonate hydroxide hydrate, and calcium aluminium carbonate hydroxide hydrate were destroyed to amorphous structure compounds which mainly contained calcium and/or aluminium components (Fig 5.10, b).

For the second set of adsorption experiments, two samples after the first set of adsorption processes (CA1 and CA3 after adsorption in 1 g/l $CuSO_4$) were extra calcined at 350°C and 950°C. These samples were labelled according to their preparation: CA3_1_950, CA1_1_950, CA1_1_350, CA3_1_350. It should be emphasized that after the first adsorption process, thermal regeneration/activation products showed high adsorption capacity. It was found out that after 60 min of adsorption, the highest amount of Cu^{2+} ions (96 mg Cu^{2+}/g (96%)) and SO_4^{2-} anions (142 mg SO_4^{2-}/g (95%)) was adsorbed by extra calcined at 950°C adsorbent CA1 after the first set of adsorption processes (CA1_1_950). A similar tendency was observed during the adsorption process by adsorbent CA3 extra calcined at 950°C after the first set of adsorption processes (CA3_1_950). It was determined that Cu^{2+} ions (95 mg Cu^{2+}/g) and SO_4^{2-} anions (135 mg SO_4^{2-}/g) were adsorbed by CA3_1_950, and this value is slightly lower in comparison to that of CA3_1_950 (Table 5.4).

Table 5.4. The amount of adsorbed Cu^{2+} ions and SO_4^{2-} anions after second adsorption cycle, mg/g

Sample	Duration, min	The amount of adsorbed Cu^{2+} ions and SO_4^{2-} anions, mg/g	
		Cu^{2+}	SO_4^{2-}
CA3_1_950	3	84	130
	20	92	134
	60	95	135
CA3_1_350	3	35	125
	20	40	126
	60	55	129
CA1_1_950	3	91	133
	20	94	136
	60	96	142
CA1_1_350	3	10	123
	20	34	125
	60	40	131

It was determined that the Cu^{2+} ions adsorption capacity of the samples was decreased by decreasing the extra calcination temperature (350°C) because after 60 min of this process, the determined values were equal: 40 mg and 55 mg Cu^{2+}ions in CA1_1_350 and CA3_1_350, respectively. The obtained data led us to conclude that the optimum condition and a high adsorption capacity (after the adsorption process involving two cycles) was determined in CA1 sample when we used 1 g/l $CuSO_4$ solution, and when the thermal regeneration/activation temperature was equal to 950°C. In order to investigate the thermal stability of the products after the second set of adsorption processes, the products were calcined for 1 h at 350 and 950°C temperatures. It was determined that at 350°C, ettringite was fully destroyed, and lower intensity diffraction maximums, which are characteristic to CuO, calcium sulphate and Ca_2CuO_3, were now detected (Fig. 5.11., a). When the temperature of calcinations was increased to 950°C, calcite fully decomposed, and compounds of amorphous structure started recrystallizing to ye'elimite, mayenite, CuO, Ca_2CuO_3, and calcium oxide (Fig. 5.11, b). The presented results showed that the finally formed calcium aluminate phases with the incorporated Cu^{2+}/SO_4^{2-} ions (adsorbent after the second adsorption process (which have a higher adsorption capacity (CA3_1_950 and CA1_1_950) were extra calcined at 350°C and 950°C) showed different crystallinity. Presumably, the above-mentioned compounds are denoted by high hydration activity and can have a positive effect on the early hydration of OPC samples. Besides, after the hydration process, the adsorbed Cu^{2+}/SO_4^{2-} ions will be immobilized in cement stone. For this reason, the test of the influence of additives (5 wt%) on the hydration process was performed: CA1_1_950_1_350; CA3_1_950_1_350; CA1_1_950_1_950; CA3_1_950_1_950 additives were mixed with pure OPC. The heat release kinetics was calculated based on the pure OPC weight.
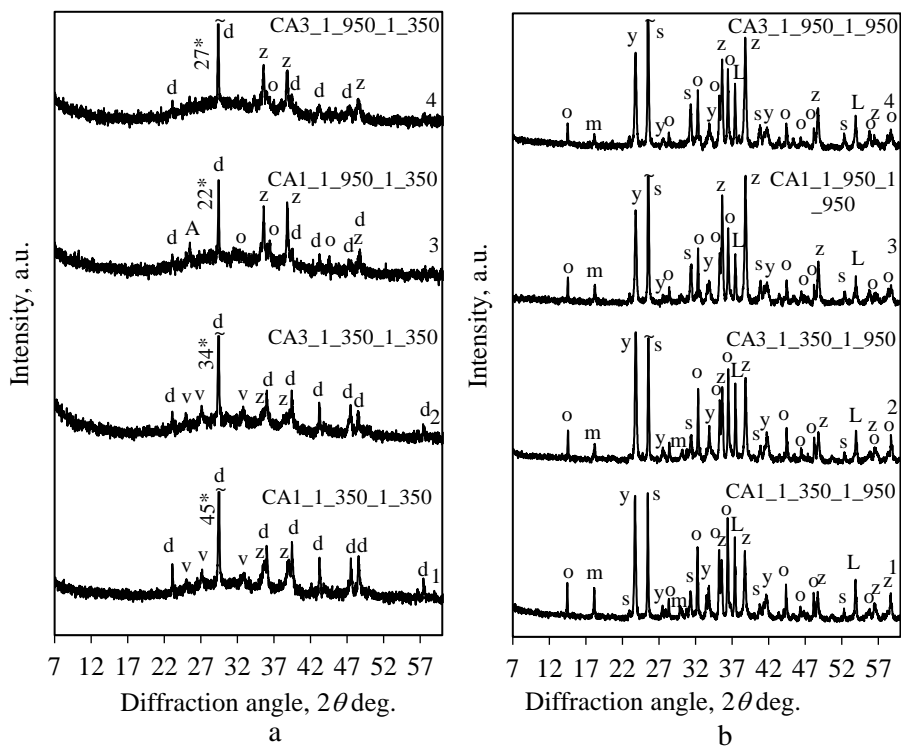
Fig. 5.11. patterns of products after second adsorption (adsorbent after the first adsorption process (1 g/l $CuSO_4$) was extra calcined at 350°C (a) and 950°C (b)) process (1 g/l $CuSO_4$) and second calcination at 350°C (a) and 950°C (b). Indexes: y – ye'elimite, L – lime, d – calcite, m – mayenite, s – calcium sulphate, z – CuO, e − ettringite, v – vaterite ($CaCO_3$), o – Ca_2CuO_3.

It was observed that all additives accelerated the first reaction (1–3 min) of cement samples because the maximum heat evolution rate increased from 0.005 W/g (pure OPC) to 0.038 W/g (OPC with CA3_1_950_1_350 additives). In the first few minutes of hydration, there was a rapid release of Ca^{2+}, OH^- and alkali ions from the cement compounds. Meanwhile, in the curves with a lower crystallinity additive, the maximum heat evolution rate increased only to 0.01–0.012. In addition, the induction period was longer; it was only extended to approximately 2.5–3 h for the sample with the above-mentioned additive in comparison with pure OPC (Fig. 5.12 b, curves 1, 4, and 5). However, the sample with the higher crystallinity additive, this period finished only after 37 h of hydration (Fig. 5.12, b, curves 2 and 3). The results demonstrate that the lower values of heat flow of the second exothermic reaction were reached in all OPC samples with additives. After 115 h of hydration, the highest quantity of the total heat (∼300 J/g) was obtained in the sample with the higher crystallinity additive, while, in the samples with lower crystallinity additive it reached only 267 J/g.
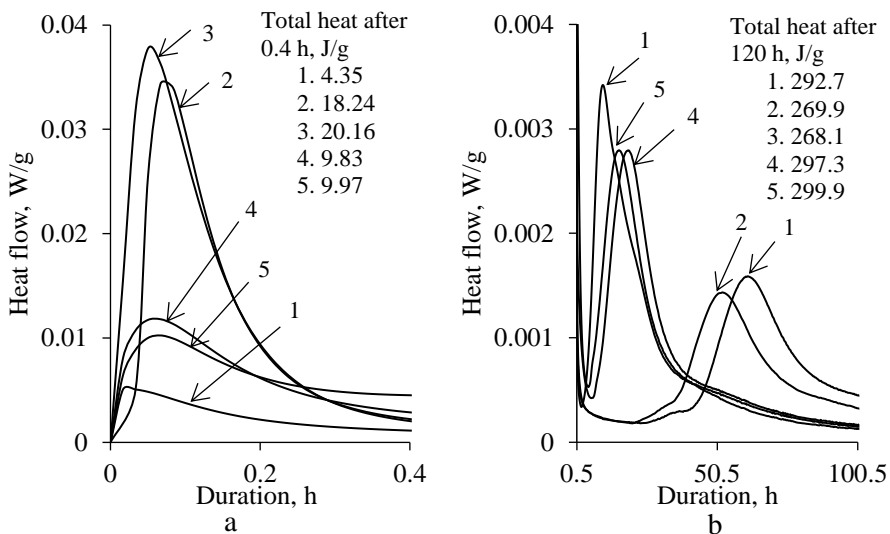
Fig. 5.12. Heat evolution rate (a, b) of pure OPC (curve 1) and OPC with different additives (5% wt.; curves 2–5) samples during the early stage of hydration. Types of additives: 2 – CA1_1_950_1_350 (curve 2); 3 – CA3_1_950_1_350 (curve 3); 4 – CA1_1_950_1_950 (curve 4); 5 – CA3_1_950_1_950 (curve 5).

The results presented here show that calcium aluminate phases with incorporated Cu^{2+}/SO_4^{2-} ions with higher crystallinity have a positive effect on the early hydration of OPC samples, and further research is needed to determine the degree of Cu^{2+}/SO_4^{2-} ions immobilization in cement stone.

5.4 Heat balance for the mayenite production process

In order to estimate the preliminary energy required for the production of mayenite, the most energy-intensive stages were modelled by Aspen Technology, Inc., i. e., the manufacturer of the chemical engineering process design software Apen Hysys and Aspen Plus. One of the most important production operations is the hydrothermal synthesis of the precursor of mayenite, katoite. The synthesis parameters were chosen according to the conditions with the highest yield of katoite: a mixture of calcium oxide and aluminium oxide with a molar ratio of CaO/Al2O3= 2,8, when the isothermal retention time is 4 hours in an immiscible suspension with a water/solids ratio of 10 at a saturated steam temperature of 130°C. The katoite synthesis process consists of the following steps: raising the temperature to 130°C, isothermal treatment (4 h), natural cooling to room temperature. For one cycle, the initial solid raw materials required are CaO = 83.15 kg, Al_2O_3 = 166.85 kg and 3,404 kg H_2O. The design autoclave has a volume of 10,000 l.

The Aspen Hysys software was used in this phase, which allows for both static and dynamic process modelling. Reaction interactions were not evaluated because their energy value is very low. It is generally accepted that the formation of calcium hydroaluminates takes place in a liquid medium, which is directly influenced by the solubility of the starting intermediates and diffusion processes. Simulated

28

hydrothermal reactor/autoclave (Fig. 5.13). The material flow in this model is based on a mixture of katoite (ID No. 200002) and water (CAS No. 7732-18-5) from the Aspen database, using the Fluid Packages – Solid system of thermodynamic equations, which is designed to simulate solid state processes.
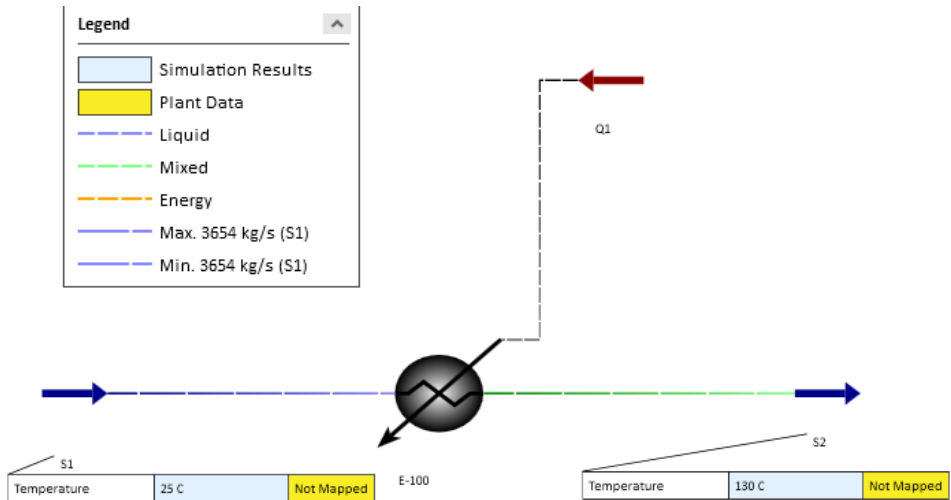

Fig. 5.13. Principle diagram of the autoclave, modelled in Aspen HYSYS environment, where: S1 – initial raw material flow; S2 – product flow; E-100 – autoclave; Q1 – process energy flow

The calculations are carried out using three different models: the first one develops a static model, which estimates the amount of energy needed to reach the required isothermal holding temperature (between 25°C and 130°C) under ideal conditions (without considering losses). The calculations showed that the energy required to achieve this process is 423.1 kW/cycle. The second is a dynamic model that evaluates the relationship between energy loss (heat loss) and the geometrical dimensions of the autoclave during temperature rise. In this model, an additional energy consumption of 7.16 kW (per cycle) was found to be needed to compensate for these heat losses. The third dynamic model is designed to estimate the amount of additional energy that needs to be fed into the system in order to maintain isothermal conditions, i.e. to compensate for heat losses during the isothermal maintenance mode, with value of 50.6 kW/cycle.

Thus, after autoclaving, the synthesised katoite is intensively mixed with the water in the medium to form a homogeneous slurry and fed into a drum centrifuge, where the excess moisture is removed, reducing the moisture content to 15%, and then fed into a dryer. Many manufacturers offer centrifuges with a total energy requirement varying from 18 to 24 kW/cycle, depending on the manufacturer. Thus, for this process, filtration in a centrifuge, the maximum energy consumption (24 kW/cycle).

The number of autoclaves and their operating mode will be such that 24 cycles can be performed/produced per day.

5.5 Conclusions

1. It was found that after 1–72 h of isothermal retention ($CaO/Al_2O_3=1.7$ at 130°C), the synthesis products are dominated by a mixture of calcium monocarboaluminate and katoite. The formation of calcium monocarboaluminate has been experimentally shown to occur during drying of the sample. The synthesis product ($CaO/Al_2O_3=2.8$, 4 hours at 130°C) was found to be dominated by katoite. The impurities of calcium monocarboaluminate and boehmite are observed as the duration of the hydrothermal reaction increases. A further increase in the CaO/Al_2O_3 ratio (2.9–3.2) has a positive effect on the intensity of the diffraction peaks of portlandite and calcium monocarboaluminate under all the conditions studied.

2. Calcium monocarboaluminate has been shown to completely decompose at ~150°C to form calcium oxide, aragonite, and gibbsite. The subsequent thermal decomposition of the latter 2 compounds is multistep, with the final stable products being CaO and Al_2O_3.

3. The S_{BET} value for synthetic katoite ($CaO/Al_2O_3=2.8$, 4 hours at 130°C) is 9.23 m^2/g. It remains stable up to 275°C and fully recrystallises at 350°C into a mixture of mayenite and portlandite. At 550°C, the portlandite completes its decomposition and the crystallinity and S_{BET} value of the mayenite decrease slightly. At 900°C, the intensity of the diffraction peaks of mayenite and calcium oxide increases and the S_{BET} of the product increases to 24.55 m^2/g.

4. The additive of mayenite derivatives has a positive effect on the early stage of the hydration of the Portland cement and as the content increases from 2.5 to 7.5%, the amount of heat released, the degree of gypsum reaction and the amount of ettringite produced increase consistently. Also, this additive, obtained under different conditions, has an influence on its hydration mechanism at the end of the wetting period, since it is only at 550°C that the mayenite obtained reacts with the ettringite and the water to form a new exothermic reaction.

5. The adsorption capacity of the mayenite derivatives for Cu^{2+} and SO_4^{2-} ions depends both on their combustion temperature and on the initial concentration of the copper sulphate solution. The highest total (192 mg/g; 93 mg/g Cu^{2+} + 98 mg/g SO_4^{2-}) ions were found to be adsorbed by the mayenite obtained at 900°C at the highest initial copper sulphate concentration (5 g Cu^{2+}/l). Meanwhile, the highest amount of copper ions (100 mg/g) was adsorbed by the mayenite obtained at 350°C at an initial copper sulphate solution concentration of 1 g Cu^{2+}/l. After the adsorption process, katoite, ettringite, and partial carbonisation products were identified in all samples, and copper

sulphate hydroxide was also formed when the concentration of the copper sulphate solution was increased to 3–5 g Cu^{2+}/l. After sorption and additional heat treatment at 350°C, it was found that the katoite completely recrystallised into mayenite.

6. After a first adsorption process and additional thermal activation, the products obtained were found to have a high adsorption capacity for Cu^{2+} and SO_4^{2-} ions in copper sulphate solution (1 g Cu^{2+}/l). After the adsorption process, it was found that the sample activated at 950°C adsorbed the highest amount of Cu^{2+} ions (96 mg Cu^{2+}/g) and SO_4^{2-} anions (142 mg SO_4^{2-}/g (95 %)). After the re-adsorption process, ettringite predominates in all samples analysed.

7. The total energy required for the hydrothermal treatment (4 hours isothermal holding at 130°C) to synthesise 333 kg of katoite per cycle is calculated to be 481 kW/cycle after taking into account the heat losses. After synthesis, the final drying and thermal decomposition is carried out in a fluidised bed reactor fed with air (9,000 kg/h, 10.7 bar and 417°C) at the lowest temperature for the formation of the mayenite (350°C), with an energy required to pressurise the air flow of 1,006 kW/cycle. Meanwhile, at the maximum temperature for the formation of mayenite (900°C), the process requires a temperature of 1,001°C and and air flow rate of 8,702 kg/h, which requires 2,572 kW/cycle of energy to heat and pressurise.

4. IŠVADOS

1. Nustatyta, kad po 1–72 val. izoterminio išlaikymo (CaO/Al_2O_3=1,7, esant 130 °C) sintezės produktuose vyrauja kalcio monokarboaliuminato ir katoito mišinys. Eksperimentiškai įrodyta, kad kalcio monokarboaliuminato susidarymas vyksta bandinio džiovinimo metu. Ištirta, kad sintezės produkte (CaO/Al_2O_3=2,8, 4 val., esant 130 °C) vyrauja katoitas. Pailginus hidroterminės reakcijos trukmę matomos kalcio monokarboaliuminato bei bemito priemaišos. Tolimesnis CaO/Al_2O_3 santykio didėjimas (2,9-3,2) turi teigiamą įtaką portlandito ir kalcio monokarboaliuminato difrakcinių smailių intensyvumui visomis tirtomis sąlygomis.

2. Ištirta, kad kalcio monokarboaliuminatas visiškai suskyla ~150 °C temperatūroje susidarant kalcio oksidui, aragonitui ir gipsitui. Pastarųjų 2-jų junginių tolesnis terminis skilimas yra daugiapakopis, o galutiniai stabilūs produktai yra CaO ir Al_2O_3.

3. Sintetinio katoito (CaO/Al_2O_3=2,8, 4 val., esant 130 °C) S_{BET} vertė yra lygi 9,23 m^2/g. Jis išlieka stabilus iki 275 °C temperatūros, o esant 350 ºC visiškai pereina į majenito bei portlandito mišinį. 550 ºC temperatūroje baigia skilti portlanditas, o majenito kristališkumas ir S_{BET} vertė šiek tiek sumažėja. 900 °C temperatūroje gerokai padidėja majenito ir kalcio oksido difrakcinių smailių intensyvumas bei produkto S_{BET} – net iki 24,55 m^2/g.

4. Majenito darinių priedas turi teigiamos įtakos ankstyvajai portlandcemenčio hidratacijos stadijai, o jo kiekį didinant nuo 2,5 iki 7,5%, išsiskyrusios šilumos kiekis, gipso sureagavimo laipsnis bei susidarančio etringito kiekis nuosekliai didėja. Taip pat šio priedo prigimtis turi įtakos jo hidratacijos mechanizmui pasibaigus drėkinimo periodui, nes tik 550 °C temperatūroje gautas majenitas reaguoja su etringitu bei vandeniu vykstant naujai egzoterminei reakcijai.

5. Majenito darinių geba adsorbuoti Cu^{2+} ir SO_4^{2-} jonus priklauso tiek nuo jų degimo temperatūros, tiek nuo pradinės vario sulfato tirpalo koncentracijos. Nustatyta, kad didžiausią bendrą (192 mg/g; 93 mg/g Cu^{2+} + 98 mg/g SO_4^{2-}) jonų kiekį adsorbavo 900 °C temperatūroje gautas majenitas esant didžiausiai pradinei vario sulfato koncentracijai (5 g Cu^{2+}/l). O didžiausią vario jonų kiekį (100 mg/g) adsorbavo 350 °C temperatūroje gautas majenitas, kai pradinio vario sulfato tirpalo koncentracija – 1 g Cu^{2+}/l. Po adsorbcijos proceso visuose bandiniuose identifikuoti katoitas, etringitas ir dalinės karbonizacijos produktai, o vario sulfato tirpalo koncentraciją padidinus iki 3–5 g Cu^{2+}/l, susidaro ir vario sulfato hidroksidas. Nustatyta, kad po sorbcijos ir papildomo terminio apdorojimo 350 °C temperatūroje katoitas visiškai persikristalizuoja į majenitą.

6. Nustatyta, kad po pirmojo adsorbcijos proceso ir papildomos terminės aktyvacijos gauti produktai pasižymi didele geba adsorbuoti Cu^{2+} ir SO_4^{2-} jonus vario sulfato tirpale (1 g Cu^{2+}/l). Nustatyta, kad po adsorbcijos proceso didžiausią Cu^{2+} jonų (96 mg Cu^{2+}/g) ir SO_4^{2-} anijonų (142 mg SO_4^{2-}/g (95 %))

kiekį adsorbuoja 950 °C temperatūroje aktyvuotas bandinys. Po pakartotinės adsorbcijos visuose tirtuose bandiniuose vyrauja etringitas.

7. Apskaičiuotas bendras hidroterminio apdorojimo (4 val. izoterminio išlaikymo 130 ºC temperatūroje) metu reikalingas energijos kiekis sintetinant 333 kg katoito vieno ciklo metu, įvertinus šilumos nuostolius jis yra 481 kW/ciklui. Po sintezės katoito galutinis džiovinimas bei jo terminis skilimas vykdomas verdančio sluoksnio reaktoriuje, į kurį, esant mažiausiai (350 °C) majenito gavimo temperatūrai, tiekiamas (9000 kg/h, 10,7 bar. ir 417 °C) oras (oro srauto suslėgimui reikalinga energija 1006 kW/ciklui). Esant didžiausiai (900 °C) majenito gavimo temperatūrai, procesui pasiekti reikalingas 1001 °C ir 8702 kg/h oro debitas, kuriam pašildyti ir suslėgti yra reikalingas 2572 kW/ciklui energijos kiekis.

LITERATŪROS SĄRAŠAS

1. Jensen TR, Christensen AN, Hanson JC. Hydrothermal transformation of the calcium aluminum oxide hydrates $CaAl_2O_4 \cdot 10H_2O$ and $Ca_2Al_2O_5 \cdot 8H_2O$ to $Ca_3Al_2(OH)_{12}$ investigated by in situ synchrotron X-ray powder diffraction. Cem Concr Res. 2005;35(12):2300-9.

2. López FA, Martín MI, Alguacil FJ, Sergio Ramírez M, González JR. Synthesis of calcium aluminates from non-saline aluminum dross. Materials. 2019;12(11):1837.

3. Ukrainczyk N, Matusinović T. Thermal properties of hydrating calcium aluminate cement pastes. Cem Concr Res. 2010;40(1):128-36.

4. Meddah MS, Zitouni S, Belâabes S. Effect of content and particle size distribution of coarse aggregate on the compressive strength of concrete. Constr Build Mater. 2010;24(4):505-12.

5. Zheng Y, Wang C, Zhou S, Xiong G. Hydration of $C_{12}A_7$-based cement (Ternal EP) in a mix with precipitated calcium carbonate. Constr Build Mater. 2022;357:129370.

6. Zhang D, Pan X, Yu H, Zhai Y. Mineral transition of calcium aluminate clinker during high-temperature sintering with low-lime dosage. Journal of Materials Science & Technology. 2015;31(12):1244-50.

7. Abolhasani A, Nazarpour H, Dehestani M. The fracture behavior and microstructure of calcium aluminate cement concrete with various water-cement ratios. Theor Appl Fract Mech. 2020;109:102690.

8. Nehring J, Neubauer J, Berger S, Goetz-Neunhoeffer F. Acceleration of OPC by CAC in binary and ternary systems: The role of pore solution chemistry. Cem Concr Res. 2018;107:264-74.

9. Schlesinger ME. Aluminum recycling. CRC press; 2013.

10. Mironova EY, Ermilova MM, Orekhova NV, Tolkacheva AS, Shkerin SN, Yaroslavtsev AB. Transformations of Ethanol on Catalysts Based on Nanoporous Calcium Aluminate–Mayenite $(Ca_{12}Al_{14}O_{33})$ and Mayenite Doped by Copper. Nanotechnologies in Russia. 2017;12(11-12):597-604.

11. Ruszak M, Inger M, Witkowski S, Wilk M, Kotarba A, Sojka Z. Selective N_2O removal from the process gas of nitric acid plants over ceramic $12CaO \cdot 7Al_2O_3$ catalyst. Catalysis letters. 2008;126(1-2):72-7.

12. de Vasconcellos LMR, Camporês KL, de Alcântara Abdala JM, Vieira MN, de Oliveira IR. Biological and microbiological behavior of calcium aluminate cement-based blend for filling of bone defects. J Mater Sci Mater Med. 2020;31(1):10.

13. Moraes PCd, Marques ICdS, Basso FG, Rossetto HL, Pires-de-Souza FdCP, Costa CAdS, et al. Repair of bone defects with chitosan-collagen biomembrane and scaffold containing calcium aluminate cement. Braz Dent J. 2017;28(3):287-95.

14. Primus C, Gutmann JL, Tay FR, Fuks AB. Calcium silicate and calcium aluminate cements for dentistry reviewed. J Am Ceram Soc. 2022;105(3):1841-63.

15. Čolović B, Janković O, Živković S, Žižak Ž, Žižak IB, Jokanović V. A new endodontic mixture based on calcium aluminate cement obtained by hydrothermal synthesis. Ceram Int. 2019;45(7):9211-8.

16. Almeida LHS, Moraes RR, Morgental RD, Cava SS, Rosa WLO, Rodrigues P, et al. Synthesis of silver-containing calcium aluminate particles and their effects on a MTA-based endodontic sealer. Dental Materials. 2018;34(8):e 214-23.

17. El-Hamid A, Radwan MM, Abo-Almaged HH. In Vitro Bioactivity Study of Calcium Aluminate/Calcium Phosphate. Interceram-International Ceramic Review. 2019;68(1):36-43.

18. Hermansson L. A review of nanostructured Ca-aluminate based biomaterials within odontology and orthopedics. Journal of the Korean Ceramic Society. 2018;55(2):95-107.

19. Engqvist H, Schultz-Walz J, Loof J, Botton GA, Mayer D, Phaneuf MW, et al. Chemical and biological integration of a mouldable bioactive ceramic material capable of forming apatite in vivo in teeth. Biomaterials. 2004;25(14):2781-7.

20. Shepherd ES, Rankin GA, Wright FE. ART. XXXII.-The Binary Systems of Alumina with Silica, Lime and Magnesia. American Journal of Science (1880-1910). 1909;28(166):293.

21. Lagerqvist K, Wallmark S, Westgren A. Röntgenuntersuchung der System $CaO \cdot Al_2O_3$ und $SrO \cdot Al_2O_3$. Zeitschrift für anorganische und allgemeine Chemie. 1937;234(1):1-16.

22. Filonenko NE, Lavrov IV. Fusion of mullite. Doklady Akad. Nauk SSSR; 1953.

23. De Vries RC, Roth WL. Critical evaluation of the literature data on beta alumina and related phases: I, phase equilibria and characterization of beta alumina phases. J Am Ceram Soc. 1969;52(7):364-9.

24. Lind M. Mechanism and kinetics of transformation of alumina inclusions in steel by calcium treatment 2006.

25. Hussain A, Mehmood S, Rasool MN, Aryal S, Rulis P, Ching WY. Electronic structure, mechanical, and optical properties of $CaO \cdot Al_2O_3$ system: a first principles approach. Indian Journal of Physics. 2016;90(8):917-29.

26. Gobbo L, Sant'Agostino L, Garcez L. C_3A polymorphs related to industrial clinker alkalies content. Cem Concr Res. 2004;34(4):657-64.

27. Nwankwo CO, Bamigboye GO, Davies IE, Michaels TA. High volume Portland cement replacement: A review. Constr Build Mater. 2020;260:120445.

28. Marchon D, Flatt RJ. Mechanisms of cement hydration. In: Science and technology of concrete admixtures. Elsevier; 2016. p. 129-45.

29. Schmidt A, Lerch M, Eufinger J, Janek J, Tranca I, Islam MM, et al. Chlorine ion mobility in Cl-mayenite ($Ca_{12}Al_{14}O_{32}Cl_2$): An investigation combining high-temperature neutron powder diffraction, impedance spectroscopy and quantum-chemical calculations. Solid State Ionics. 2014;254:48-58.

30. Kim SW, Matsuishi S, Nomura T, Kubota Y, Takata M, Hayashi K, et al. Metallic state in a lime − alumina compound with nanoporous structure. Nano letters. 2007;7(5):1138-43.

31. Savuto E, Navarro RM, Mota N, Di Carlo A, Bocci E, Carlini M, et al. Steam reforming of tar model compounds over Ni/Mayenite catalysts: effect of Ce addition. Fuel. 2018;224:676-86.

32. Cucciniello R, Intiso A, Castiglione S, Genga A, Proto A, Rossi F. Total oxidation of trichloroethylene over mayenite ($Ca_{12}Al_{14}O_{33}$) catalyst. Applied Catalysis B: Environmental. 2017;204:167-72.

33. Intiso A, Martinez-Triguero J, Cucciniello R, Proto A, Palomares AE, Rossi F. A novel synthetic route to prepare high surface area mayenite catalyst for TCE oxidation. Catalysts. 2019;9(1):27.

34. Shengwen T, Wenzhi YU, Zhou W, Li Y, Hubao A. No title. Method of manufacturing semiconductor material from mayenite. 2020.

35. Liu X, Liu Y, Yan D, Zhu H, Liu C, Xu C, et al. Single-phased white-emitting $12CaO·7Al_2O_3$:Ce^3, Dy 3 phosphors with suitable electrical conductivity for field emission displays. Journal of Materials Chemistry. 2012;22(33):16839-43.

36. Park H, Sung S, Park C, Won J. Influence of a $C_{12}A_7$ mineral-based accelerator on the strength and durability of shotcrete. Cem Concr Res. 2008;38(3):379-85.

37. Tanaka S, Ozaki I, Kunimoto T, Ohmi K, Kobayashi H. Blue emitting $CaAl_2O_4$: Eu2 phosphors for PDP application. J Lumin. 2000;87:1250-3.

38. Ma C, Kampf AR, Connolly Jr HC, Beckett JR, Rossman GR, Smith SAS, et al. Krotite, $CaAl_2O_4$, a new refractory mineral from the NWA 1934 meteorite. Am Mineral. 2011;96(5-6):709-15.

39. Lazić B, Kahlenberg V, Konzett J, Kaindl R. On the polymorphism of $CaAl_2O_4$— structural investigations of two high pressure modifications. Solid state sciences. 2006;8(6):589-97.

40. Qi C, Spagnoli D, Fourie A. Structural, electronic, and mechanical properties of calcium aluminate cements: Insight from first-principles theory. Constr Build Mater. 2020;264:120259.

41. Aggarwal PS, Gard JA, Glasser FP, Biggar GM. Synthesis and properties of dicalcium aluminate, $2CaO·Al_2O_3$. Cem Concr Res. 1972;2(3):291-7.

42. Hayashi K, Ueda N, Hirano M, Hosono H. Effect of stability and diffusivity of extra-framework oxygen species on the formation of oxygen radicals in $12CaO·7Al_2O_3$. Solid State Ionics. 2004;173(1-4):89-94.

43. Ruszak M, Witkowski S, Pietrzyk P, Kotarba A, Sojka Z. The role of intermediate calcium aluminate phases in solid state synthesis of mayenite ($Ca_{12}Al_{14}O_{33}$). Functional Materials Letters. 2011;4(02):183-6.

44. Kahlenberg V, Fischer RX, Shaw CS. Rietveld analysis of dicalcium aluminate ($Ca_2Al_2O_5$)—A new high pressure phase with the Brownmillerite-type structure. Am Mineral. 2000;85(7-8):1061-5.

45. Singh V, Yadav M, Sharma YC. Effect of co-solvent on biodiesel production using calcium aluminium oxide as a reusable catalyst and waste vegetable oil. Fuel. 2017;203:360-9.

46. Claude V, Mahy JG, Lohay T, Tilkin RG, Micheli F, Lambert SD. Sol-gel synthesis of Ni/Al_2O_3 catalysts for toluene reforming: Support modification with alkali, alkaline earth or rare-earth dopant (Ca, K, Mg or Ce). Surfaces and Interfaces. 2020:100511.

47. Fujii K, Kondo W, Ueno H. Kinetics of Hydration of Monocaldum Aluminate. J Am Ceram Soc. 1986;69(4):361-4.

48. Gülgün MA, Popoola OO, Kriven WM. Chemical synthesis and characterization of calcium aluminate powders. J Am Ceram Soc. 1994;77(2):531-9.

49. Tian Y, Pan X, Yu H, Tu G. Formation mechanism of calcium aluminate compounds based on high-temperature solid-state reaction. J Alloys Compounds. 2016;670:96-104.

50. Shiri S, Abbasi MH, Monshi A, Karimzadeh F. Synthesis of the $CaAl_2O_4$ nanoceramic compound using high-energy ball milling with subsequent annealing. Advanced Powder Technology. 2014;25(1):338-41.

51. Amer AA, El-Didamony H, El-Sokkary TM, Wahdan MI. Synthesis and characterization of some calcium aluminate phases from nano-size starting materials. Boletín de la Sociedad Española de Cerámica y Vidrio. 2020.

52. Salah A, El-Faramawy N, Ahmed M, Farouk S. Synthesis and thermoluminescence studies of beta particle irradiated $CaAl_2O_4$. J Lumin. 2022:119461.

53. Selyunina L, Mishenina L, Belyaninova T, Botvina T. Sol-Gel Synthesis of Fluorescent Materials Based on Tricalcium Aluminate. JPhCS. 2019;1145(1):012031.

54. Mandić V, Kurajica S. The influence of solvents on sol–gel derived calcium aluminate. Materials Science in Semiconductor Processing. 2015;38:306-13.

55. Jeong Y, Balamurugan C, Lee D. Enhanced CO_2 gas-sensing performance of ZnO nanopowder by La loaded during simple hydrothermal method. Sensors Actuators B: Chem. 2016;229:288-96.

56. Ho C, Wei C, Lin S, Ding S. Calcium silicate cements prepared by hydrothermal synthesis for bone repair. Ceram Int. 2016;42(7):9183-9.

57. Meller N, Kyritsis K, Hall C. The hydrothermal decomposition of calcium monosulfoaluminate 14-hydrate to katoite hydrogarnet and β-anhydrite: An in-situ synchrotron X-ray diffraction study. Journal of Solid State Chemistry. 2009;182(10):2743-7.

58. Ríos CA, Williams CD, Fullen MA. Hydrothermal synthesis of hydrogarnet and tobermorite at 175 °C from kaolinite and metakaolinite in the $CaO–Al_2O_3–SiO_2–H_2O$ system: A comparative study. Appl Clay Sci. 2009;43(2):228-37.

59. Meller N, Hall C, Kyritsis K, Giriat G. Synthesis of cement based $CaO–Al_2O_3–SiO_2–H_2O$ (CASH) hydroceramics at 200 and 250 °C: Ex-situ and in-situ diffraction. Cem Concr Res. 2007;37(6):823-33.

60. Karimi MA, Ranjbar M. Hydrothermal synthesis and characterization of $CaCO_3$ nanostructure. Synthesis and Reactivity in Inorganic, Metal-Organic, and Nano-Metal Chemistry. 2016;46(5):635-7.

61. Li C, Hirabayashi D, Suzuki K. Synthesis of higher surface area mayenite by hydrothermal method. Mater Res Bull. 2011;46(8):1307-10.

62. Khan K, Li J, Zou W, Xu W, Yang Y, Song W. Low temperature synthesis of nano porous $12CaO·7Al_2O_3$ powder by hydrothermal method. Journal of Wuhan University of Technology-Mater.Sci.Ed. 2016;31(6):1201-5.

63. Hewlett P. Lea's chemistry of cement and concrete. Elsevier; 2003.

64. Parrott LJ, Geiker M, Gutteridge WA, Killoh D. Monitoring Portland cement hydration: comparison of methods. Cem Concr Res. 1990;20(6):919-26.

65. Powers TC. Structure and physical properties of hardened Portland cement paste. J Am Ceram Soc. 1958;41(1):1-6.

66. Kakali G, Tsivilis S, Aggeli E, Bati M. Hydration products of C_3A, C_3S and Portland cement in the presence of $CaCO_3$. Cem Concr Res. 2000;30(7):1073-7.

67. De Rojas MS, Luxan MP, Frías M, Garcia N. The influence of different additions on portland cement hydration heat. Cem Concr Res. 1993;23(1):46-54.

68. Joseph S, Skibsted J, Cizer Ö. A quantitative study of the C_3A hydration. Cem Concr Res. 2019;115:145-59.

69. Plank J, Hirsch C. Impact of zeta potential of early cement hydration phases on superplasticizer adsorption. Cem Concr Res. 2007;37(4):537-42.

70. Matschei T, Lothenbach B, Glasser FP. The role of calcium carbonate in cement hydration. Cem Concr Res. 2007;37(4):551-8.

71. Shang X, Ye G, Zhang Y, Li H, Hou D. Effect of micro-sized alumina powder on the hydration products of calcium aluminate cement at 40 °C. Ceram Int. 2016;42(13):14391-4.

72. Luz AP, Pandolfelli VC. $CaCO_3$ addition effect on the hydration and mechanical strength evolution of calcium aluminate cement for endodontic applications. Ceram Int. 2012;38(2):1417-25.

73. Mostafa NY, Zaki ZI, Abd Elkader OH. Chemical activation of calcium aluminate cement composites cured at elevated temperature. Cement and Concrete Composites. 2012;34(10):1187-93.

74. Klaus S, Buhr A, Schmidtmeier D, Kuiper S, Goetz-Neunhoeffer F. Hydration of calcium aluminate cement phases Ca and Ca2 in refractory applications. Proceeding of UNITECR ; 2015.

75. Winnefeld F, Lothenbach B. Hydration of calcium sulfoaluminate cements—Experimental findings and thermodynamic modelling. Cem Concr Res. 2010;40(8):1239-47.

76. Gong L, Lin Z, Ning S, Sun J, Shen J, Torimoto Y, et al. Synthesis and characteristics of the $C_{12}A_7$-O^- nanoparticles by citric acid sol–gel combustion method. Mater Lett. 2010;64(11):1322-4.

77. Shi C, Qu B, Provis JL. Recent progress in low-carbon binders. Cem Concr Res. 2019;122:227-50.

78. Telesca A, Marroccoli M, Tomasulo M, Valenti GL, Dieter H, Montagnaro F. Low-CO_2 cements from fluidized bed process wastes and other industrial by-products. Combustion Sci Technol. 2016;188(4-5):492-503.

79. Telesca A, Marroccoli M, Winnefeld F. Synthesis and characterisation of calcium sulfoaluminate cements produced by different chemical gypsums. Advances in cement research. 2019;31(3):113-23.

80. Carmona-Quiroga PM, Montes M, Pato E, Fernández-Jiménez A, Blanco-Varela MT. Study on the activation of ternesite in $CaO \cdot Al_2O_3$ and $12CaO \cdot 7Al_2O_3$ blends with gypsum for the development of low-CO_2 binders. J Clean Prod. 2021;291:125726.

81. Bizzozero J, Scrivener KL. Limestone reaction in calcium aluminate cement–calcium sulfate systems. Cem Concr Res. 2015;76:159-69.

82. Navarro-Blasco I, Duran A, Sirera R, Fernández JM, Alvarez JI. Solidification/stabilization of toxic metals in calcium aluminate cement matrices. J Hazard Mater. 2013;260:89-103.

83. Zhang M, Yang C, Zhang Z, Zhu X, Huang W, Zhao M, et al. Understanding the binding and leaching of Cr (VI) in calcium aluminate cement based solidified/stabilized pastes. Constr Build Mater. 2020;262:120040.

84. Chen L, Wang Y, Wang L, Zhang Y, Li J, Tong L, et al. Stabilisation/solidification of municipal solid waste incineration fly ash by phosphate-enhanced calcium aluminate cement. J Hazard Mater. 2021;408:124404.

85. Wang T, Zhang P, Wu D, Sun M, Deng Y, Frost RL. Effective removal of zinc (II) from aqueous solutions by tricalcium aluminate (C_3A). J Colloid Interface Sci. 2015;443:65-71.

86. Zhang P, Ouyang S, Li P, Sun Z, Ding N, Huang Y. Ultrahigh removal performance of lead from wastewater by tricalcium aluminate via precipitation combining flocculation with amorphous aluminum. J Clean Prod. 2020;246:118728.

87. Zhang P, Zeng X, Wen X, Yang C, Ouyang S, Li P, et al. Insights into efficient removal and mechanism for ammonium from aqueous solution on tricalcium aluminate. Chem Eng J. 2019;366:11-20.

88. Zhao Y, Niu Y, Hu X, Xi B, Peng X, Liu W, et al. Removal of ammonium ions from aqueous solutions using zeolite synthesized from red mud. Desalination and Water Treatment. 2016;57(10):4720-31.

89. Uğurlu M, Karaoğlu MH. Adsorption of ammonium from an aqueous solution by fly ash and sepiolite: Isotherm, kinetic and thermodynamic analysis. Microporous and Mesoporous Materials. 2011;139(1-3):173-8.

90. Wang X, Qiao B, Li S, Li J. Using natural Chinese zeolite to remove ammonium from rainfall runoff following urea fertilization of a paddy rice field. Environmental Science and Pollution Research. 2016;23(6):5342-51.

91. Luukkonen T, Sarkkinen M, Kemppainen K, Rämö J, Lassi U. Metakaolin geopolymer characterization and application for ammonium removal from model solutions and landfill leachate. Appl Clay Sci. 2016;119:266-76.

92. Radfarnia HR, Sayari A. A highly efficient CaO-based CO_2 sorbent prepared by a citrate-assisted sol–gel technique. Chem Eng J. 2015;262:913-20.

93. Zhou Z, Xu P, Xie M, Cheng Z, Yuan W. Modeling of the carbonation kinetics of a synthetic CaO-based sorbent. Chemical Engineering Science. 2013;95:283-90.

94. Angeli SD, Martavaltzi CS, Lemonidou AA. Development of a novel-synthesized Ca-based CO_2 sorbent for multicycle operation: Parametric study of sorption. Fuel. 2014;127:62-9.

95. Bian Z, Li Y, Wu S, Yan X, Zhao J, Wang Z. SO_2 removal performances of Al- and Mg-modified carbide slags from CO_2 capture cycles at calcium looping conditions. Journal of Thermal Analysis and Calorimetry. 2021;144(4):1187-97.

96. Li Y, Shi L, Liu C, He Z, Wu S. Studies on CO_2 uptake by $CaO/Ca_3Al_2O_6$ sorbent in calcium looping cycles. Journal of Thermal Analysis and Calorimetry. 2015;120(3):1519-28.

97. Zhang M, Peng Y, Sun Y, Li P, Yu J. Preparation of $CaO–Al_2O_3$ sorbent and CO_2 capture performance at high temperature. Fuel. 2013;111:636-42.

98. Jing J, Li T, Zhang X, Wang S, Feng J, Turmel WA, et al. Enhanced CO_2 sorption performance of $CaO/Ca_3Al_2O_6$ sorbents and its sintering-resistance mechanism. Appl Energy. 2017;199:225-33.

99. Aguilar FG, Garcia LFR, Pires-de-Souza FCP. Biocompatibility of new calcium aluminate cement (EndoBinder). J Endod. 2012;38(3):367-71.

100. Jacobovitz M, Vianna ME, Pandolfelli VC, Oliveira IR, Rossetto HL, Gomes BP. Root canal filling with cements based on mineral aggregates: an in vitro analysis of bacterial microleakage. Oral Surgery, Oral Medicine, Oral Pathology, Oral Radiology, and Endodontology. 2009;108(1):140-4.

101. Faris A, Engqvist H, Lööf J, Ottosson M, Hermansson L. In vitro bioactivity of injectable ceramic orthopaedic cements. Key Engineering Materials; Trans Tech Publ; 2006.

102. Lööf J, Faris A, Hermansson L, Engqvist H. In Vitro Biomechanical Testing of Two Injectable Materials for Vertebroplasty in Different Synthetic Bones. Key Engineering Materials; Trans Tech Publ; 2008.

103. Oliveira IR, Pandolfelli VC, Jacobovitz M. Chemical, physical and mechanical properties of a novel calcium aluminate endodontic cement. Int Endod J. 2010;43(12):1069-76.

104. Castro-Raucci LMSd, Oliveira IRd, Teixeira LN, Rosa AL, Oliveira PTd, Jacobovitz M. Effects of a novel calcium aluminate cement on the early events of the progression of osteogenic cell cultures. Braz Dent J. 2011;22(2):99-104.

105. Silva E, Accorsi-Mendonça T, Almeida J, Ferraz C, Gomes B, Zaia AA. Evaluation of cytotoxicity and up-regulation of gelatinases in human fibroblast cells by four root canal sealers. Int Endod J. 2012;45(1):49-56.

106. Parreira RM, Andrade TL, Luz AP, Pandolfelli VC, Oliveira IR. Calcium aluminate cement-based compositions for biomaterial applications. Ceram Int. 2016;42(10):11732-8.

107. Liao S, Yao R, Chen X, Wang G, Zheng F. Characteristics, thermodynamics, and preparation of nanocaged $12CaO \cdot 7Al_2O_3$ and its derivatives. International Journal of Applied Ceramic Technology. 2016;13(5):844-55.

108. Zhang J, Zhang Z, Wang T, Hao W. Preparation and characterization of a new long afterglow indigo phosphor $Ca_{12}Al_{14}O_{33}$: Nd, Eu. Mater Lett. 2003;57(26-27):4315-8.

109. Li J, Huang F, Wang L, Wang Z, Yu S, Torimoto Y, et al. Mechanistic Features for Hydroxyl Anion Emission from the Modified $12CaO \cdot 7Al_2O_3$ Surface. The Journal of Physical Chemistry B. 2005;109(30):14599-603.

110. Schmidt A, Boysen H, Senyshyn A, Lerch M. New findings on N-mayenite and a new kind of anion substituted mayenite: $Ca_{12}Al_{14}O_{32}(NO_2)_2$. Zeitschrift für Kristallographie-Crystalline Materials. 2014;229(6):427-34.

111. Xue X, Li H, Lu L, Liu Q, Mi X, Bai Z, et al. Effect of the anion on the luminescence properties of Bi_3 -doped X-mayenite (X= O, F, Cl) phosphors. Mater Res Bull. 2021;139:111283.

112. Rudradawong C, Ruttanapun C. Combined effects of Mg reducing and Sn doping on the electrical conductivity of polycrystalline $Ca_{12}Al_{14}O_{33}$ mayenite. Applied Physics A. 2019;125(4):252.

113. Weber S, Schunk SA. Reply to Inoue et al. Comment on "Weber et al. Mayenite-Based Electride $C_{12}A_7e^-$: A Reactivity and Stability Study. Catalysts 2021, 11, 334". Catalysts. 2021;11(10):1155.

114. Matović B, Nikolić MG, Prekajski-Đorđević MD, Dmitrović S, Luković JM, Maletaškić J, et al. Luminescence Properties Of Eu^3 Doped Mayenite Under High Pressure. Journal of Innovative Materials in Extreme Conditions. 2020;1(1):12-8.

115. Jeevaratnam J, Glasser FP, Glasser LD. Anion Substitution and Structure of $12CaO \cdot 7Al_{22}O_{13}$. J Am Ceram Soc. 1964;47(2):105-6.

116. Li J, Huang F, Wang L, Yu SQ, Torimoto Y, Sadakata M, et al. High Density Hydroxyl Anions in a Microporous Crystal:$[Ca_{24}Al_{28}O_{64}]_4 \cdot 4(OH^-)$. Chemistry of materials. 2005;17(10):2771-4.

117. Dekel DR. Review of cell performance in anion exchange membrane fuel cells. J Power Sources. 2018;375:158-69.

118. Weitkamp RF, Neumann B, Stammler H, Hoge B. Generation and Applications of the Hydroxide Trihydrate Anion,$[OH(OH_2)_3]^-$, Stabilized by a Weakly Coordinating Cation. Angewandte Chemie International Edition. 2019;58(41):14633-8.

119. Yang S, Kondo JN, Hayashi K, Hirano M, Domen K, Hosono H. Partial oxidation of methane to syngas over promoted $C_{12}A_7$. Applied Catalysis A: General. 2004;277(1-2):239-46.

120. Hosono H, Abe Y. Occurrence of superoxide radical ion in crystalline calcium aluminate $12CaO \cdot 7Al_2O_3$ prepared via solid-state reactions. Inorg Chem. 1987;26(8):1192-5.

121. Hayashi K, Hirano M, Matsuishi S, Hosono H. Microporous Crystal $12CaO \cdot 7Al_2O_3$ Encaging Abundant O-Radicals. J Am Chem Soc. 2002;124(5):738-9.

122. Watauchi S, Tanaka I, Hayashi K, Hirano M, Hosono H. Crystal growth of Ca12Al14O33 by the floating zone method. J Cryst Growth. 2002;237:801-5.

123. Matsuishi S, Toda Y, Miyakawa M, Hayashi K, Kamiya T, Hirano M, et al. High-Density Electron Anions in a Nanoporous Single Crystal:$[Ca_{24}Al_{28}O_{64}]_4 (4e^-)$. Science. 2003;301(5633):626-9.

124. Kim SW, Hosono H. Synthesis and properties of $12CaO \cdot 7Al_2O_3$ electride: review of single crystal and thin film growth. Philosophical Magazine. 2012;92(19-21):2596-628.

125. Salasin JR, Rawn C. Structure property relationships and cationic doping in $[Ca_{24}Al_{28}O_{64}]4$ framework: a review. Crystals. 2017;7(5):143.

126. Khan K, Tareen AK, Aslam M, Thebo KH, Khan U, Wang R, et al. A comprehensive review on synthesis of pristine and doped inorganic room temperature stable mayenite electride,$[Ca_{24}Al_{28}O_{64}] (e^-)4$ and its applications as a catalyst. Progress in Solid State Chemistry. 2019;54:1-19.

127. Volodin AM, Kenzhin RM, Kapishnikov AV, Komarovskikh AY, Vedyagin AA. Aluminothermic Synthesis of Dispersed Electrides Based on Mayenite: XRD and EPR Study. Materials. 2022;15(24):8988.

128. Li F, Zhang X, Zhang J. One-step fabrication of inorganic $[Ca_{24}Al_{28}O_{64}]_4 (4e^-)$ from transition metal and oxide compound precursors by reactive sintering. Ceram Int. 2019;45(17):23830-5.

129. Langlar W, Aeimbhu A, Limsuwan P, Ruttanapun C. Microwave-assisted biosynthesis of $C_{12}A_7$ nanopowders from Aloe Vera leaf extract. Journal of the Ceramic Society of Japan. 2020;128(6):322-8.

130. Li F, Zhang X, Liu H. Calciothermic synthesis of inorganic $[Ca_{24}Al_{28}O_{64}]_4$ $(4e^-)$ electride from solid-derived precursor. Vacuum. 2019;169:108880.

131. Khan K, Tareen AK, Elshahat S, Yadav A, Khan U, Yang M, et al. Facile synthesis of a cationic-doped $[Ca_{24}Al_{28}O_{64}]_4$ $(4e^-)$ composite via a rapid citrate sol–gel method. Dalton Transactions. 2018;47(11):3819-30.

132. Chang Y, Chang P, Lee Y, Lee T, Lai Y, Chen S. Morphological and structural evolution of mesoporous calcium aluminate nanocomposites by microwave-assisted synthesis. Microporous and mesoporous materials. 2014;183:134-42.

133. Manera C, Perondi D, Barbieri RA, Barcellos T, Godinho M. Ultrasonication-promoted synthesis of Ni/mayenite for catalytic reforming of biomass tar. Ultrason Sonochem. 2020;67:105165.

134. Koehler A, Neubauer J, Goetz-Neunhoeffer F. How $C_{12}A_7$ influences the early hydration of calcium aluminate cement at different temperatures. Cem Concr Res. 2022;162:106972.

135. Tolkacheva AS, Shkerin SN, Plaksin SV, Vovkotrub EG, Bulanin KM, Kochedykov VA, et al. Synthesis of dense ceramics of single-phase mayenite $(Ca_{12}Al_{14}O_{32})$ O. Russian Journal of Applied Chemistry. 2011;84(6):907-11.

136. Hayashi K, Hirano M, Hosono H. Thermodynamics and Kinetics of Hydroxide Ion Formation in $12CaO \cdot 7Al_2O_3$. The Journal of Physical Chemistry B. 2005;109(24):11900-6.

137. Wang Q, Yang J, Yan P. Influence of initial alkalinity on the hydration of steel slag. Science China Technological Sciences. 2012;55(12):3378-87.

138. Edmonds RN, Majumdar AJ. The hydration of $12CaO \cdot 7Al_2O_3$ at different temperatures. Cem Concr Res. 1988;18(3):473-8.

139. Koplík J, Tomala L, Novotný R. Hydration of calcium aluminate phases at different temperatures. Advanced Materials Research; Trans Tech Publ; 2014.

140. He Z, Li Y. The Influence of Mayenite Employed as a Functional Component on Hydration Properties of Ordinary Portland Cement. Materials. 2018;11(10):1958.

141. Meza-Trujillo I, Mary A, Pietrzyk P, Sojka Z, Gaigneaux EM. Nature and role of Cu (II) species in doped $C_{12}A_7$ catalysts for soot oxidation. Applied Catalysis B: Environmental. 2022;316:121604.

142. Shuvarakova EI, Ilyina EV, Stoyanovskii VO, Veselov GB, Bedilo AF, Vedyagin AA. Exploration of optical, redox, and catalytic properties of vanadia-mayenite nanocomposites. Journal of Composites Science. 2022;6(10):308.

143. Meza-Trujillo I, Devred F, Gaigneaux EM. Production of high surface area mayenite $(C_{12}A_7)$ via an assisted solution combustion synthesis (SCS) toward catalytic soot oxidation. Mater Res Bull. 2019;119:110542.

144. Liu X, Li L, Sun H, Wen G, Wang D, Ren S, et al. NiW catalyst modified with $C_{12}A_7$-H^- and its promotion to hydrogenation selectivity of hydrodesulfurization. Fuel. 2021;290:120037.

145. Kitano M, Kanbara S, Inoue Y, Kuganathan N, Sushko PV, Yokoyama T, et al. Electride support boosts nitrogen dissociation over ruthenium catalyst and shifts the bottleneck in ammonia synthesis. Nature communications. 2015;6(1):1-9.

146. Herce C, Cortés C, Stendardo S. Numerical simulation of a bubbling fluidized bed reactor for sorption-enhanced steam methane reforming under industrially relevant conditions: Effect of sorbent (dolomite and $CaO-Ca_{12}Al_{14}O_{33}$) and operational parameters. Fuel Process Technol. 2019;186:137-48.

147. Di Carlo A, Bocci E, Zuccari F, Dell'Era A. Numerical investigation of sorption enhanced steam methane reforming process using computational fluid dynamics Eulerian− Eulerian code. Ind Eng Chem Res. 2010;49(4):1561-76.

148. Baltakys K, Eisinas A, Doneliene J, Dambrauskas T, Sarapajevaite G. The impact of Al_2O_3 amount on the synthesis of CASH samples and their influence on the early stage hydration of calcium aluminate cement. Ceram Int. 2019;45(2):2881-6.

149. Eisinas A, Doneliene J, Baltakys K, Urbutis A. Hydrothermal synthesis of calcium aluminium hydrate-based adsorbent for the removal of CO_2. Journal of Thermal Analysis and Calorimetry. 2018;131(1):537-44.

150. Piekkari K, Isteri V, Ohenoja K, Illikainen M. Hazardous industrial filter sludge immobilization with mayenite and gypsum. J Clean Prod. 2023:135873.

151. Xin D, Chai X, Zhao W. Hybrid cement-assisted dewatering, solidification and stabilization of sewage sludge with high organic content. Journal of Material Cycles and Waste Management. 2016;18(2):356-65.

152. Paul B, Chang W. Mayenite-to-hydrocalumite transformation for the removal of chloride from salinized groundwater and the recycling potential of spent hydrocalumite for chromate removal. Desalination. 2020;474:114186.

153. Alex TC, Kumar R, Roy SK, Mehrotra SP. Mechanically induced reactivity of gibbsite: Part 1. Planetary milling. Powder Technol. 2014;264:105-13.

154. Sun M, Jin H, Guo X, Wang S, Bi J, Ji Z, et al. Precipitation and in-situ surface modification of calcium carbonate in synthetic seawater: Polymorph control, crystallization kinetics, and hydrophobic vaterite preparation. Journal of Environmental Chemical Engineering. 2023;11(3):110019.

155. Trezza MA, Lavat AE. Analysis of the system $3CaO \cdot Al_2O_3$–$CaSO_4 \cdot 2H_2O$–$CaCO_3$–H_2O by FT-IR spectroscopy. Cem Concr Res. 2001;31(6):869-72.

156. Cheng P, Liu Y, Yang L, Wang X, Chi Y, Yuan H, et al. Adsorption and recovery of phosphate from aqueous solution by katoite: Performance and mechanism. Colloids Surf Physicochem Eng Aspects. 2022;655:130285.

157. Shen SC, Chen Q, Chow PS, Tan GH, Zeng XT, Wang Z, et al. Steam-assisted solid wet-gel synthesis of high-quality nanorods of boehmite and alumina. The Journal of Physical Chemistry C. 2007;111(2):700-7.

158. Jiménez A, Rives V, Vicente MA. Thermal study of the hydrocalumite–katoite–calcite system. Thermochimica Acta. 2022;713:179242.

159. Zhu B, Fang B, Li X. Dehydration reactions and kinetic parameters of gibbsite. Ceram Int. 2010;36(8):2493-8.

160. Trombetta M, Armaroli T, Alejandre AG, Solis JR, Busca G. An FT-IR study of the internal and external surfaces of HZSM5 zeolite. Applied Catalysis A: General. 2000;192(1):125-36.

161. Delhomme F, Ambroise J, Limam A. Effects of high temperatures on mortar specimens containing Portland cement and GGBFS. Mater Struct. 2012;45:1685-92.

162. Saleh HM, El-Sheikh SM, Elshereafy EE, Essa AK. Performance of cement-slag-titanate nanofibers composite immobilized radioactive waste solution through frost and flooding events. Constr Build Mater. 2019;223:221-32.

163. Torréns-Martín D, Fernández-Carrasco L, Martínez-Ramírez S. Hydration of calcium aluminates and calcium sulfoaluminate studied by Raman spectroscopy. Cem Concr Res. 2013;47:43-50.

164. Lothenbach B, Zajac M. Application of thermodynamic modelling to hydrated cements. Cem Concr Res. 2019;123:105779.

165. Georget F, Lothenbach B, Wilson W, Zunino F, Scrivener KL. Stability of hemicarbonate under cement paste-like conditions. Cem Concr Res. 2022;153:106692.

CURRICULUM VITAE

Vardas Pavardė: Kristina Vasiliauskienė
El. paštas: kristina.ruginyte@gmail.com

Išsilavinimas:
2012–2016 Taikomosios chemijos bakalauras, Kauno technologijos universitetas
2016–2018 Chemijos inžinerijos magistras, Kauno technologijos universitetas
2019–2023 doktorantūra chemijos inžinerijos srityje, Kauno technologijos universitetas

Profesinė patirtis:
2018
Technologė UAB „Plastmė"
2018 – dabar
Technologė I. Kriščiūno firma IGIS
2020 – 2024 04 01
Jaunesnioji mokslo darbuotoja projekte „Mažakalcio cemento dvistadijinė sintezė, jo struktūra ir savybės", Kauno technologijos universitetas

Web of Science duomenų bazėje indeksuotuose leidiniuose su cituojamumo rodikliu

1. Eisinas, Anatolijus; Vasiliauskiene, Kristina. Effect of Cu^{2+}/SO_4^{2-} ions concentration on the adsorption capacity of synthetic mayenite, its application for secondary adsorption process and utilization in cement samples // Ceramics international. Oxford : Elsevier. ISSN 0272-8842. eISSN 1873-3956. 2022

2. Baltakys, Kestutis; Eisinas, Anatolijus; Vasiliauskiene, Kristina; Palou, Martin T.; Dambrauskas, Tadas. The effect of calcined mayenite on the hydration of ordinary Portland cement // Ceramics international. Oxford : Elsevier. ISSN 0272-8842. eISSN 1873-3956. 2022

3. Eisinas, A.; Ruginyte, K.; Baltakys, K.; Demcak, S.; Dambrauskas, T.; Balintova, M.; Stevulova, N. Cu^{2+} ion adsorption by synthetic mayenite and its thermal stability // Ceramics international. Oxford : Elsevier. ISSN 0272-8842. eISSN 1873-3956. 2020, vol. 46, iss. 18, pt. B, p. 29429-29435

Mokslinės konferencijos:

1. Ruginytė, K.; Eisinas, A. The formation and thermal stability of Mayenite // NBCM 2020: international conference on nanostructured bioceramic materials, 1-3 December 2020, Vilnius, Vilnius University: conference book. Vilnius : Vilnius Univerity Press, 2020. ISBN 9786090705575. p. 69.

2. Ruginytė, Kristina; Eisinas, Anatolijus. The effect of synthetic katoite additive on the hydration of calcium aluminate cement // 6th Central and Eastern European conference on thermal analysis and calorimetry (CEEC-TAC6) and 15th Mediterranean conference on calorimetry and thermal analysis (Medicta2021), 20-24 July 2021, Split, Croatia: book of abstracts / A. Rotaru, M. Erceg (eds). București : SITECH, 2021, PS3.012. ISBN 9786061178612. p. 208

3. Eisinas, Anatolijus; Ruginytė, Kristina; Dambrauskas, Tadas; Baltakys, Kestutis. The effect of Cu^{2+} ions concentration on the adsorption capacity of synthetic mayenite and its thermal stability // 6th Central and Eastern European conference on thermal analysis and calorimetry (CEEC-TAC6) and 15th Mediterranean conference on calorimetry and thermal analysis (Medicta2021), 20-24 July 2021, Split, Croatia: book of abstracts / A. Rotaru, M. Erceg (eds). București : SITECH, 2021, PS3.011. ISBN 9786061178612. p. 207.

4. Ruginytė, Kristina; Eisinas, Anatolijus. The influence of thermal synthesis parameters on mayenite structure // Advanced materials and technologies: book of abstracts of 23rd international conference-school, 23- 27 August 2021, Palanga, Lithuania. Kaunas : Kaunas university of technology. ISSN 2669-1930. 2021, B-P116, p. 148.

5. Ruginyte, Kristina; Eisinas, Anatolijus. The influence of mayenite additive on the early stage hydration of portland cement // Chemistry and chemical technology: 16th international conference of Lithuanian Chemical Society, 24 September 2021, Vilnius, Lithuania: book of abstracts. Vilnius : National Center for Physical Sciences and Technology. 2021, P023, p. 37.

6. Eisinas, Anatolijus; Vasiliauskiene, Kristina; Dambrauskas, Tadas; Baltakys, Kestutis. The effect of calcination temperature on mayenite hydration properties // 1st Central and Eastern European conference on physical chemistry and materials science (CEEC-PCMS1), 26-30 July 2022, Split, Croa: book of abstracts / editors: M. Erceg, A. Rotaru, L. Vrsalovic. Craiova : Sitech, 2022, PS2.18. ISBN 9786061181643. p. 160.

7. Vasiliauskiene, Kristina; Eisinas, Anatolijus. Formation of katoite during hydrothermal synthesis in the mixtures with CaO/Al_2O_3 molar ratio 2.8-3.2 // 1st Central and Eastern European conference on physical chemistry and materials science (CEEC-PCMS1), 26-30 July 2022, Split, Croa: book of abstracts / editors: M. Erceg, A. Rotaru, L. Vrsalovic. Craiova : Sitech, 2022, PS2.22. ISBN 9786061181643. p. 164.

8. Vasiliauskiene, K.; Eisinas, A. Hydration properties of mayenite and gypsum mixture // FIM 2022: International conference "Functional inorganic materials 2022": abstract book. Vilnius : Vilnius university press, 2022. eISBN 9786090707777. p. 80. (Vilnius university proceedings, eISSN 2669-0233 ; vol. 29).

PADĖKA